THE JOURNAL OF PHYSICAL CHEMISTRY C

Article

Cite This: J. Phys. Chem. C XXXX, XXX, XXX−XXX

pubs.acs.org/JPCC

Reversible Aggregation of Covalently Cross-Linked Gold Nanocrystals by Linker Oxidation

Zhongyue Luan,[†] Trenton Salk,[‡] Alex Abelson,[†] Stephanie Jean,[§] and Matt Law*[,†,∥]

[†]Department of Materials Science & Engineering, University of California, Irvine, Irvine, California 92697, United States

[‡]Department of Physics and Astronomy, University of California, Irvine, Irvine, California 92697, United States

[§]Department of Chemistry, College of Saint Benedict, St. Joseph, Minnesota 56374, United States

[∥]Department of Chemistry, University of California, Irvine, Irvine, California 92697, United States

Supporting Information

ABSTRACT: Covalent cross-linking of colloidal gold nanocrystals (Au NCs) with dithiol molecules is normally considered to be an irreversible self-assembly process. Left unchecked, dithiol-mediated aggregation results in the uncontrolled formation of polymeric NC-dithiolate precipitates. Here we demonstrate the reversible assembly and disassembly of dithiolate-linked precipitates and colloidal aggregates of Au NCs by oxidizing the dithiolate linkers with ozone. Destruction of the linkers results in the complete depolymerization of the NC aggregates/precipitates to re-form stable aqueous colloids of individual Au NCs with retention of the original NC size distribution. The process is repeatable by adding additional dithiol to reinitiate aggregation, although some irreversible fusion of the NCs occurs in subsequent cycles. This method for reversible self-assembly of covalently cross-linked Au NCs is simple, clean, reproducible, and effective for a variety of linkers. Extending reversibility to covalently bound NC assemblies creates new possibilities in plasmonic sensing and catalysis.

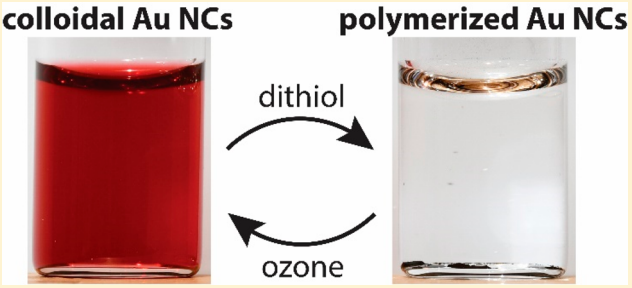

INTRODUCTION

The demonstration of stable alkanethiolate-capped colloidal gold nanocrystals by Brust et al.[1] launched a wave of research on surface functionalization strategies to control the assembly of plasmonic metal nanocrystals (NCs).[2−7] Plasmon coupling between proximate gold or silver NCs causes large shifts in the localized surface plasmon resonance (LSPR) and the creation of nm^3-scale regions of strongly enhanced electromagnetic field strength (hot spots).[8] Due to these dramatic near- and far-field optical effects, assemblies of colloidal gold and silver NCs are of significant interest for many applications, notably chemical sensing, disease detection and treatment, metamaterials, and photocatalysis. Particular effort has focused in two areas: (i) the development of highly sensitive and selective colorimetric chemical sensors based on the aggregation or size/shape changes of Au and Ag NCs[9,10] and (ii) the rational assembly of Au and Ag NC dimers with optimized electromagnetic hot spots for surface-enhanced Raman spectroscopy (SERS) at the single-molecule limit.[11] Schemes that enable reversible NC aggregation with fine control of the aggregate size distribution are important for these and other potential uses of plasmonic metal NCs.

One fundamental degree of control is the ability to reverse the NC aggregation process using an external stimulus. Reversibility is interesting because it allows for dynamic tuning of the aggregates, real-time response to stimuli, resetting of the NC assembly to its initial state, and reuse of the NCs. Reversible NC aggregation has been demonstrated using the full gamut of noncovalent interactions, including hydrogen bonding, solvophobicity, electrostatic and van der Waals forces, and π-effects. Reversible assembly schemes have been based on biomolecular recognition of DNA,[12,13] aptamer-analyte,[14,15] antibody−antigen,[16] and protein−substrate complexes,[17,18] stimuli-responsive polymer coatings triggered by pH,[19,20] temperature,[21,22] light,[23,24] solvent polarity,[25,26] and solution composition,[27] hydrogen bonding between small molecules,[28−30] metal ion complexation,[31,32] host−guest chemistry,[33,34] charge-transfer complex formation,[35] control of electrostatic stabilization by ionic strength,[36] temperature,[37] photoisomerization of azobenzene-functionalized ligands,[38−40] and partial exchange with nonbridging ligands,[41,42] and light-driven thermophoresis[43] and plasmofluidic trapping.[44] In contrast, there are few examples of reversible aggregation of metal NCs cross-linked with covalent bonds. He et al. employed photodimerization and photocleavage of a coumarin-functionalized thiol ligand to achieve the reversible covalent cross-linking of Au NCs.[45] Guarise and co-workers used a dithiol linker with a chemically cleavable ester backbone to

Received: July 22, 2019
Revised: August 31, 2019
Published: September 3, 2019

DOI: 10.1021/acs.jpcc.9b06976
J. Phys. Chem. C XXXX, XXX, XXX−XXX

depolymerize aggregates of Au NCs.[46] Displacement of multidentate thioether linkers by monothiols was shown by Lim et al. to result in disassembly of Au NC aggregates.[47] While effective, these approaches rely on specialized or relatively weak covalent linkers. A general method for reversible self-assembly of covalently cross-linked Au NCs has not been demonstrated.

Control of the size distribution of colloidal NC aggregates is a second major goal of metal NC assembly. The simplest and in many ways most important aggregate is the NC dimer. Despite its simplicity, the deterministic fabrication of NC dimers has proven a tremendous challenge, and no method has yet been developed for the quantitative conversion of a dispersion of individual colloidal NCs into NC dimers. The two main approaches for assembling colloidal NC dimers are asymmetric functionalization and arrested aggregation. The former approach utilizes assembly at solid−liquid[48−52] or liquid−liquid interfaces[53,54] to break symmetry and selectively make dimers, but processing is complicated and dimer yields are usually low. Arrested aggregation involves stopping the NC aggregation process at an early stage of polymerization in order to produce a dispersion of NC oligomers that contains a high percentage of dimers. This is typically achieved by using dilute reactants to ensure slow polymerization and/or terminating the polymerization by encapsulating the NCs with polymers,[55−58] silica,[59,60] or phospholipids.[61] Aggregation initiators include DNA,[62,63] biotin−streptavadin,[18,64] amide bond formation,[65,66] dithiol linkers,[58,67−72] salt,[60,73,74] antisolvents,[75,76] and neutral nonbridging ligands.[77,78] Since NC aggregation inevitably results in a distribution of aggregate sizes (monomers, dimers, and higher oligomers), postfabrication separation is often used to enrich the dimer content.[58,79,80] In addition to asymmetric functionalization and arrested aggregation, several types of novel lithography have also been used to make NC dimers for SERS studies.[81−83]

While exploring routes to the deterministic fabrication of colloidal Au NC dimers, we discovered that precipitates of Au NCs covalently cross-linked by dithiols[84] can be completely depolymerized and redispersed in water by brief exposure to ozone. Ozone has been previously used to induce reversible shifts of the LSPR of Au NCs[85,86] and to oxidize organic ligands from colloidal[87] and surface-supported Au NCs.[88,89] We show here that ozone depolymerizes the NC precipitates by oxidizing and cleaving the dithiolate linkers to weakly bound sulfonates that exchange with free citrate in solution to yield dispersions of citrate-capped NCs. The process works with many thiol linkers, including oligo ethylene glycol dithiols and alkane dithiols of various length and water solubility. The NC size and shape distributions are largely preserved. Complete redispersion of "hard crashed" bulk NC precipitates occurs in minutes to days depending on the amount of dithiol used to affect the polymerization. The precipitation−redispersion cycle can be repeated multiple times by sequential addition of dithiol linker and ozone. Ozone-mediated linker oxidation is a simple, clean, and general approach to the reversible assembly of covalently cross-linked Au NCs.

METHODS

Materials. All chemicals were used as received unless otherwise noted. 18.2 MΩ water (Millipore Milli-Q Gradient) was used throughout the study. Hydrogen tetrachloroaurate(III) trihydrate ($HAuCl_4 \cdot 3H_2O$, 99.99%) was purchased from Alfa Aesar. Trisodium citrate dihydrate (>99.8%) was purchased from MP Biomedical. Hexa(ethylene glycol) dithiol (HEGDT, >97%), 2,2′-(ethylenedioxy)diethanethiol (EDD, 95%), pentaerythritol tetrakis(3-mercaptopropionate) (PTMP, 95%), 1,6-hexanedithiol (HDT, 99.5%), sodium hydroxide (NaOH, 97%), 3-mercaptopropionic acid (MPA, 99%), 11-mercaptoundecanoic acid (MUDA, 95%), 16-mercaptohexadecanoic acid (MHDA, 99%), 3-(trimethylsilyl)-1-propanesulfonic acid sodium salt (DSS sodium salt, 97%), biphenyl-4,4′-dithiol (DBDT, 95%), poly(ethylene glycol) (PEG, average M_n = 400), anhydrous ethanol (>99.5%), and deuterium oxide (D_2O, 99.9 atom % D) were purchased from Sigma-Aldrich. Hexa(ethylene glycol) monothiol (HEGMT, 97%) was purchased from BroadPharm. Tetrahydrofuran (THF, 99.9%) was purchased from Acros Organics. Oxygen (>99.993%), argon (>99.999%), and nitrogen (>99.999%) were purchased from Praxair. Fresh aqua regia was prepared by mixing hydrochloric acid (HCl, 36.5−38.0%, ACS grade, J.T. Baker) and nitric acid (HNO_3, 69.0−70.0%, ACS grade, J.T. Baker) in a molar ratio of 3:1. Nitric acid (TraceMetal grade, Fisher Scientific) was double distilled for ICP-MS analysis. Methanol (LC−MS grade) for mass spectrometry was purchased from J.T. Baker.

Gold Nanocrystal Synthesis. Citrate-capped gold nanocrystals were synthesized using a published method.[90] Briefly, 1 mL of a 25 mM aqueous solution of $HAuCl_4 \cdot 3H_2O$ was added by pipet to 150 mL of 2.2 mM aqueous trisodium citrate dihydrate in a 250 mL round-bottom flask under 1000 rpm stirring at 100 °C. The solution color changed from yellow to dark blue and then light red. After a reaction time of 15 min, the solution was cooled to 90 °C and 1 mL of 60 mM aqueous trisodium citrate dihydrate was injected into the flask, followed by 1 mL of a 25 mM aqueous solution of $HAuCl_4 \cdot 3H_2O$ 2 min later. This sequential injection of the two precursors was repeated 14 times (at 30 min intervals) at 90 °C to increase the NC diameter. Finally, the reaction was quenched with an ice bath and the NC dispersion was stored without purification at 2−8 °C. On the basis of the precursor concentrations and volumes used, the NC dispersion contains 19.61 mM sodium ion and 8.38 mM chloride ion.

Thiol-Mediated Aggregation. In a glass vial at room temperature, 1.000 mL of the as-made Au NC colloid was diluted with 0−999 μL of water. Then, 1−1000 μL of a 10 mM aqueous solution of HEGDT was added to the vial to yield a total volume of 2.000 mL. Final values of [HEGDT]/[NC] were 2000 to 2 000 000, as described in the text. EDD, PTMP, and HDT were added in the same way as HEGDT. Each vial was then tightly capped and allowed to sit unstirred on the benchtop in ambient conditions.

Ozone-Mediated NC Redispersion. To redisperse the aggregated/precipitated NCs, the output of an ozone generator (Enaly model 5000BF) fed with oxygen gas was bubbled at 0.2 L/min into an open glass vial of aggregated/precipitated NCs for 5 min under sonication (Branson model 1510) at room temperature (unless otherwise noted). Steady-state ozone concentrations in the gas stream and solution were estimated to be at least 1 mM and 350 μM, respectively. The vial was then sparged with argon at 0.2 L/min for 1 min to remove the residual ozone, capped, and stored in ambient conditions (unless otherwise noted). Since ozonation of high concentrations of HEGDT (i.e., [HEGDT]/[NC] ≥ 1 000 000) lowers the pH enough to dissolve the NCs, 10 μL (20 μL) of a 1 M aqueous solution of NaOH was added to samples with [HEGDT]/[NC] = 1 000 000 (2 000 000) to adjust the pH to

DOI: 10.1021/acs.jpcc.9b06976
J. Phys. Chem. C XXXX, XXX, XXX−XXX

~12.0 before ozonation. After ozonation, the pH of these samples decreased to ~6.0. Alternatively, washing these precipitates to remove the large excess of HEGDT and then ozonating the samples in pure water also gave rapid and complete NC redispersion.

Monothiol-Mediated NC Redispersion. To test redispersion of the precipitated NCs by thiol self-exchange, a large excess of a monothiol ([monothiol]/[NC] = 4 000 000) was added to the original supernatant of hard-crashed NC precipitates prepared as described above using [HEGDT]/[NC] = 4000. Monothiol additions were 200 μL of 100 mM of HEGMT in water, MPA in water, MUDA in ethanol, or MHDA in ethanol. After addition of the monothiol, the vial was tightly sealed and sonicated for 5 min, sparged with argon for 1 min, and stored for 7 days at room temperature. Alternatively, the samples were sonicated for 12 h at 75 °C. MHDA and MUDA formed micellar emulsions in water, so these samples were passed through a 0.2 μM PTFE syringe filter (28145-495, VWR) to remove the micelles and reduce light scattering prior to acquiring optical extinction spectra.

Characterization Techniques. Optical extinction spectra (λ = 400−800 nm) were acquired in quartz cuvettes (Spectrocell model R-4010) on a PerkinElmer Lambda 950 spectrophotometer. The concentration of dissolved ozone was quantified using the X^1A_1 to $^1B_2$ transition at 260 nm (ε = 2992 M^{-1} cm^{-1}).[91] Transmission electron microscopy (TEM) was performed on a JEOL JEM-2100F TEM operating at 200 keV. Scanning electron microscopy (SEM) was performed on an FEI Magellan 400 XHR SEM operating at 10 keV and 50 pA. TEM and SEM samples were prepared by pipetting a droplet of NC colloid onto a lacey carbon copper grid (Ted Pella model 01824) or Si substrate, respectively. After 10 s, the droplet was blown off the grid/substrate with a stream of argon to avoid the artificial formation of NC aggregates during slow drying. pH measurements were made on stirred samples every 3 s using a calibrated pH meter (Oakton model PC2700). ^{1}H NMR data were collected in pure D_2O or a 1:1 mixture of the NC dispersion and D_2O in precision NMR tubes (Wilmad model 528-PP-7) using a Bruker DRX500 spectrometer (500 MHz, BBO probe) with 16 scans at a delay time of 20 s. Absolute concentrations of citrate, HEGDT, and other species were determined with an internal reference (DSS sodium salt). The pulsed field gradient technique was used to suppress the H_2O signal. Use of water suppression had no effect on the quantification results. ^{1}H NMR results for HEGDT and 5 min ozonated HEGDT are as follows.

HEGDT: ^{1}H NMR (D_2O, δ in ppm) 3.70 (16H, s, HEG backbone), 3.67 (4H, t, J = 6.24 Hz, −O-C$\underline{H}_2$−CH_2−SH), 2.73 (4H, t, J = 6.25 Hz, −O−CH_2−C$\underline{H}_2$-SH).

Ozonated HEGDT: ^{1}H NMR (D_2O, δ in ppm) 8.22 (1H, s, $\underline{H}$COOH) 3.89 (4H, t, J = 6.72 Hz, −O-C$\underline{H}_2$−CH_2−SO_3H), 3.70 (16H, s, HEG backbone), 3.20 (4H, t, J = 6.70 Hz, −O−CH_2−C$\underline{H}_2$−SO_3H).

The Au NC concentration was determined by inductively coupled plasma mass spectrometry (ICP-MS). Known volumes of Au NC colloid were added to fresh aqua regia, diluted with double-distilled nitric acid as needed, and immediately measured on a Nu AttoM ES HR-ICP-MS spectrometer using the low-resolution peak jump method with 15 cycles of 500 sweeps and 500 μs dwells per peak. A noble metals standard (VHG Labs SM40-100) was used to construct a calibration curve, and an internal standard (VHG Labs LIS3-100) was used to correct for drift and matrix-related artifacts. On the basis of the measured Au concentration of 0.41 g/L and the known size of the NCs (from TEM images), we find [NC] = 4.99 nM in the as-made Au NC colloid. Control experiments performed on the supernatant of centrifuged NC colloids showed that the dissolved Au concentration was below the ICP-MS detection limit, meaning that effectively all of the Au atoms are contained in the NCs, with negligible free Au in these samples.

Solution small-angle X-ray scattering (SAXS) measurements of as-made and ozone-redispersed Au NC colloids were performed at beamline 7.3.3 of the Advanced Light Source (ALS) at Lawrence Berkeley National Laboratory using monochromatic X-rays (λ = 1.24 Å, 10 keV) with an energy bandwidth of 1%. Samples were measured in transmission geometry in 1 mm diameter quartz capillaries (Hampton Research). 2D SAXS patterns were collected on a Dectris Pilatus 2M detector at a sample−detector distance of 3504.75 mm as calibrated by a silver behenate standard in a quartz capillary. Signal was collected for 120 s. The Nika software package[92] in Igor Pro was used to azimuthally integrate (25−75°) the SAXS patterns. Particle size distribution fitting was performed with the IPG/TNNLS fitting routine in Irena assuming a spherical NC shape. Several measurements were performed across the length of the capillary to verify sample uniformity.

Attenuated total reflectance FTIR spectra were acquired with a Nicolet 6700 FTIR spectrometer equipped with a GladiATR diamond ATR module (Pike Technologies) using 128 scans at a resolution of 4 cm^{-1}. Samples were prepared by centrifuging as-made Au NC colloids, discarding the supernatant, cleaning the NCs four times in ethanol to remove free citrate and other species present in the reaction solution, and drying a droplet of the purified Au NC colloid on the ATR crystal. In situ HEGDT or citrate treatments were performed by flooding samples on the ATR crystal with 1 mL of 10 mM aqueous HEGDT or 1 M aqueous trisodium citrate for 1 h, wicking away the liquid, flooding with 1 mL of water for 30 min, and finally wicking away the water and drying the sample in a stream of nitrogen.

X-ray photoelectron spectroscopy (XPS) data of the S 2p and Au 4f regions were acquired with a Kratos AXIS Supra spectrometer using monochromatic Al Kα radiation at an X-ray power of 225 W and 40 eV pass energy (5 sweeps, 0.05 eV step size, and 500 ms dwell times). As-made and ozone-redispersed Au NC colloids were purified by centrifuge diafiltration (Amicon Ultra-15 centrifugal filter unit, UFC905024, 50 kDa cutoff) to remove solutes (e.g., citrate, salt, HEGDT ozonation products) and loosely bound ligands. Briefly, 10 mL samples of each colloid were centrifuge-filtered at 2000 rpm for 30 min. The concentrated NC colloid was then rediluted to 10 mL with water. This cycle was repeated four times to yield 10 mL batches of purified NC colloids (10^5-fold lower solute concentrations with no loss of NCs). The cleaned NCs were then concentrated and drop cast onto O_2 plasma-cleaned Si substrates (Zepto, Diener Electronics) under a stream of nitrogen. NC-HEGDT precipitates were prepared for XPS measurements by four cycles of normal centrifugation and rinsing with water, followed by drop casting and drying on Si substrates. Finally, the dried samples were carefully stamp transferred onto carbon tape (Ted Pella model 16073), which was then mounted to a Si substrate and transferred to the XPS chamber for measurement. All spectra were charge corrected using the Au $4f_{7/2}$ peak at 84.0 eV.

DOI: 10.1021/acs.jpcc.9b06976
J. Phys. Chem. C XXXX, XXX, XXX−XXX

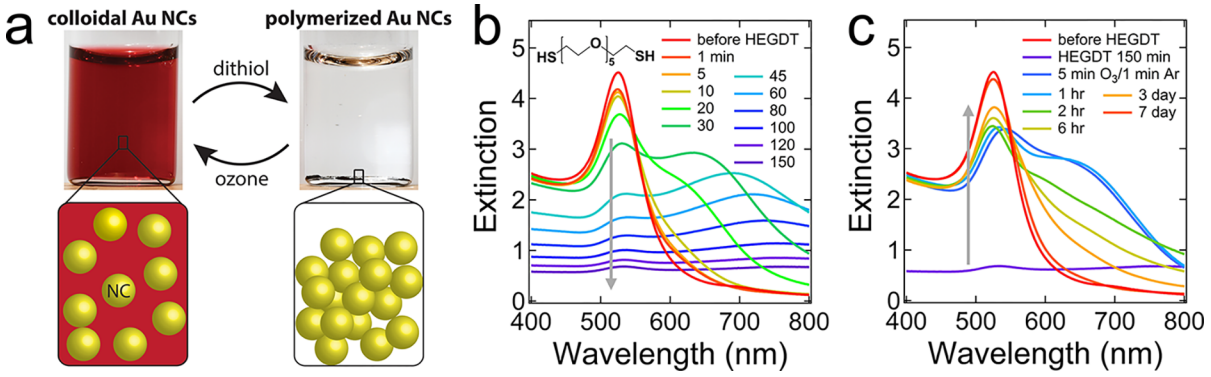

Figure 1. Redispersion of dithiolate-linked Au nanocrystal aggregates/precipitates with ozone. (a) Reaction scheme explored in this paper. Addition of excess dithiol triggers the large scale cross-linking of colloidal Au NCs in water, resulting in rapid precipitation of a NC-dithiolate polymer. Subsequent ozone bubbling depolymerizes and completely redisperses the NCs. (b) Time series of optical extinction spectra after adding aqueous hexa(ethylene glycol) dithiol (HEGDT) to the NC colloid ([HEGDT]/[NC] = 4000). The molecular structure of HEGDT is shown in the inset. (c) Spectral time series upon ozonation of the precipitated NC-HEGDT polymer using 5 min of ozone bubbling with sonication followed by a 1 min argon sparge at room temperature. See Methods for details.

Mass spectrometry data were acquired on a Waters LCT Premier TOF mass spectrometer using electrospray ionization and an MCP detector operating in positive ion mode. Aqueous samples were diluted to 10 μM with methanol. Poly(ethylene glycol) served as the internal reference.

Raman spectra were acquired on a home-built Raman microscope (λ_{ex} = 532 nm) with 10% laser power, 10 exposures per second, and 5 scans from −100 to 3200 cm^{-1}. Samples were prepared by mixing 0.75 mL of the as-made Au NC colloid, 1.15 mL of water, and 0.1 mL of 10 mM HEGDT in water or 5 mM DBDT in THF, waiting for 5 min, and then drop casting five droplets of the HEGDT- or DBDT-treated NCs onto plasma-cleaned Si substrates, rinsing the films with copious water or THF, respectively, and drying in a stream of nitrogen. Reference films of HEGDT and DBDT were prepared by drop casting and drying five droplets of 10 mM HEGDT or 5 mM DBDT solutions in water and THF, respectively.

RESULTS AND DISCUSSION

Figure 1a depicts the reversible aggregation scheme explored in this paper. The aggregation of citrate-capped colloidal gold nanocrystals in water is initiated by addition of a small-molecule dithiol linker. Covalent cross-linking of the NCs results in the formation of colloidal aggregates or bulk precipitates depending on the NC and linker concentrations, reaction time, and solution temperature. A stream of ozone and oxygen is then bubbled through the solution to reverse the aggregation and redisperse the NCs. The cycle can be repeated by adding more dithiol to reinitiate aggregation.

We use hexa(ethylene glycol) dithiol (HEGDT) as a proof-of-concept linker because oligo ethylene glycol dithiols are water-soluble, short, available in various lengths, and have small Raman scattering cross sections, making them suitable Raman-silent linkers for the fabrication of high-performance SERS dimer nanoantennae (Figure S1). Our use of HEGDT was inspired by early papers showing that monothiolated glycols yield stable water-soluble Au NCs.[93−96]

We monitored the aggregation process using optical extinction spectroscopy and transmission electron microscopy (TEM). Figure 1b shows a typical spectral time series for a 4.99 nM dispersion of 23.8 ± 4.2 nm citrate-capped Au NCs in their unpurified reaction mixture upon dilution with water and addition of aqueous HEGDT at room temperature to give initial NC and HEGDT concentrations of 2.50 nM and 10 μM, respectively (see Methods and molecular structure of HEGDT in Figure 1b). In addition to the NCs, this diluted reaction mixture contains 2.65 mM free citrate ion (as determined by nuclear magnetic resonance (NMR) spectroscopy), 4.19 mM chloride ion, 9.80 mM sodium ion, 0.29 mM acetone, 0.05 mM acetic acid, and probably various undetected organic and inorganic species, all at pH 6.0 ± 0.2 (total ionic strength of 14 ± 0.7 mM). Within minutes of adding HEGDT, the NC plasmon peak at ∼527 nm began to decrease in intensity and a broad absorbance band developed at longer wavelengths. These spectral changes are characteristic of the formation of a distribution of colloidal NC aggregates with some concurrent precipitation (Figure 1b).[97] The molar ratio of HEGDT to NCs in this experiment ([HEGDT]/[NC] = 4000) was large enough to quickly and completely precipitate the NCs (a "hard crash" of the NCs). After ∼150 min, the original ruby red NC solution had turned colorless and a powdery black precipitate rested on the bottom and sides of the vial. TEM images showed that the original well-dispersed spheroidal NCs had formed large aggregates consisting of many thousands of NCs (Figure S2). Control experiments with hexa(ethylene glycol) monothiol (HEGMT) showed no NC aggregation or precipitation even days after mixing (Figure S3), suggesting that HEGDT-induced aggregation results mainly from covalent cross-linking of the NCs by HEGDT rather than changes in NC surface charge, ligand hydrophobicity, or other factors. Due to strong covalent cross-linking by HEGDT, these NC precipitates could not be redispersed by any combination of prolonged sonication and heating (up to 100 °C) in water (at any pH) or common organic solvents.

The Au NC precipitates slowly redispersed after brief exposure to ozone (Figure 1c). Samples were bubbled with an ozone/oxygen mixture under sonication for 5 min, sparged with argon without sonication for 1 min to remove the ozone, and allowed to age on the benchtop in ambient conditions (see Methods). The dissolved ozone concentration was quantified by monitoring the strong ozone absorption band at 260 nm.[98] Using ε_{260nm} = 2992 M^{-1} cm^{-1},[91] we estimate an ozone concentration of 340−360 μM. Furthermore, the absorption spectra show that the argon purge is effective at flushing the dissolved ozone out of the solution (Figure S4). Within a

DOI: 10.1021/acs.jpcc.9b06976
J. Phys. Chem. C XXXX, XXX, XXX−XXX

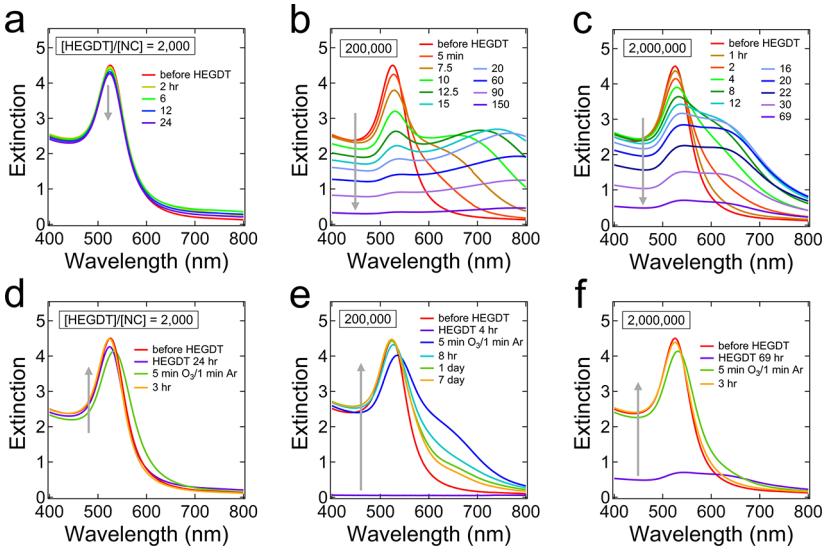

Figure 2. NC precipitation–redispersion behavior as a function of [HEGDT]/[NC]. Time series of optical extinction spectra after adding aqueous HEGDT to the NC colloid at [HEGDT]/[NC] of (a) 2000, (b) 200 000, and (c) 2 000 000. (d–f) Corresponding spectral time series upon ozonation of the NC-HEGDT oligomers/polymers.

minute of adding ozone, all of the black solid was consumed and the colorless solution turned dark blue, then gradually deep ruby red over the course of several days (Figure 1c). After ~7 days, the spectrum of the ozone-treated solution closely matched the spectrum of the original NC colloid before addition of HEGDT (λ_{max} = 528.5 and 527 nm, respectively). This is strong evidence that ozonation completely redisperses the precipitates to form a sol of individual Au NCs with a negligible fraction of dimers and larger aggregates. TEM images confirmed this conclusion (Figure S5). Size histograms compiled from the TEM images of samples before addition of HEGDT and 7 days after ozonation show that the average NC diameter and diameter distribution increased slightly from 23.8 ± 4.2 nm to 24.7 ± 7.4 nm. Solution small-angle X-ray scattering (SAXS) measurements gave very similar results (21.6 ± 3.9 nm and 22.7 ± 4.9 nm; see Figure S5). The images and histograms show that the size and shape of most of the NCs are unchanged after one precipitation–redispersion cycle. However, a small number of NCs do grow in size (visible as a tail in the size distributions), probably as a result of the occasional metallic fusion of adjacent NCs within the precipitates (Figure S5). Our finding of insignificant etching and oxidation of Au NCs by brief ozone treatment is consistent with previous reports.[85,87] The NC sols are indefinitely stable after ozonation and showed no additional spectral changes after more than 2 years of storage in ambient conditions. Moreover, ozonation sterilizes the samples and prevents the growth of fungus that often occurs in citrate-stabilized Au NC colloids (Figure S6).[99]

We used attenuated total reflectance FTIR spectroscopy to determine if HEGDT displaces citrate from the surface of our Au NCs. While thiols are believed to adsorb more strongly than citrate to colloidal Au NCs in water, the equilibrium constant for citrate–thiolate surface exchange, e.g.,

$$\text{NC-Cit}^{3-} + \text{HEGDT} \rightleftharpoons \text{NC-HEGDT}^{-} + \text{HCit}^{2-}$$

is unknown, making it difficult to estimate the relative surface coverage of thiolate and citrate during their competitive adsorption under different experimental conditions. The Shumaker-Parry group recently reported that citrate is not removed from Au NCs by treatment with excess alkyl or aryl thiols in ethanol.[100] However, while citrate is quite insoluble in ethanol, it is soluble in water. We anticipated that our use of water as solvent (enabled by the high water solubility of HEGDT) would favor citrate displacement by thiols (i.e., ligand exchange rather than coadsorption). Indeed, the ATR-FTIR data show that adsorbed citrate is easily removed by a brief rinse in pure water or treatment with aqueous HEGDT (Figure S7). Adsorbed HEGDT is strongly bound to the NCs and cannot be removed by prolonged rinsing in water or citrate solution. We conclude that HEGDT easily displaces citrate from the surface of Au NCs in water and the equilibrium constant for exchange is probably very large. We note that our observation of facile citrate desorption in pure water is at odds with Park and Shumaker-Parry, who found significant retention of adsorbed citrate after extensive rinsing of Au NCs with water at pH ~10.[101]

We found that the dithiol-to-NC ratio ([HEGDT]/[NC]) has a large effect on the extent and speed of NC aggregation and redispersion. Small ratios (<1000) cause no measurable aggregation (insignificant spectral changes even 4 days after mixing). Increasing the ratio from 1200 to 2000 resulted in mild but progressive aggregation without precipitation. For example, Figure 2a and Figure 2d show the aggregation–redispersion behavior at [HEGDT]/[NC] = 2000. Under these conditions only small colloidal aggregates form and the associated spectral changes are slight. Ozonation of these samples 1 day after HEGDT addition caused an immediate redshift of the plasmon peak from 524 to 533 nm and slow recovery to the original, pre-HEGDT spectrum in ~3 h, indicating complete redispersion of the colloidal agglomerates into individual Au NCs. Control experiments show that this fast redshift and slow recovery are caused by adsorption and desorption of ozone on the surface of the NCs rather than the deaggregation process itself (Figure S8).[85,86] The rapid redispersion (probably minutes or less) is likely facilitated by the small size of the aggregates and relatively low coverage of HEGDT linkers at this low [HEGDT]/[NC]. Larger values of [HEGDT]/[NC] caused increasingly rapid and complete NC aggregation and precipitation. We observed slight precipitation

DOI: 10.1021/acs.jpcc.9b06976
J. Phys. Chem. C XXXX, XXX, XXX–XXX

at a ratio of 2400, substantial precipitation at 2800, and full precipitation for ratios larger than ~3000.

NC redispersion is similarly fast at high [HEGDT]/[NC] values (>10^6). Under these conditions, a high HEGDT surface coverage leaves few bare gold surface atoms on each NC available for cross-linking, so the NCs have a low sticking probability and the polymerization is slow. Complete precipitation takes ~70 h at [HEGDT]/[NC] = 2 × 10^6 compared to ~2 h at [HEGDT]/[NC] = 4000 (Figure 2c and Figure 2f). Despite the slow aggregation and precipitation, redispersion is just as fast as at [HEGDT]/[NC] = 2000, as evidenced by the nearly identical series of spectra after ozonation (Figure 2d and Figure 2f). We believe that this rapid redispersion is due to a low cross-link density in NC aggregates made at high HEGDT surface coverages. When the cross-link density is low, only a small number of linkers must be broken per NC to achieve depolymerization. We also note that the slower polymerization at high HEGDT coverage confirms that the active linker is indeed HEGDT (i.e., Au−S−R−S−Au), rather than a disulfide formed by oxidative coupling of HEGDT ligands on neighboring NCs (which should result in faster polymerization at high HEGDT coverage because of the greater number of terminal thiols available for disulfide formation).

Whereas aggregation is slow and redispersion is fast at small and large dithiol-to-NC ratios, the opposite is true at intermediate ratios. At intermediate [HEGDT]/[NC] values, aggregation is fast (1−2 h) and redispersion slow (5−10 days) because the NCs have a significant coverage of both linkers and bare gold atom binding sites, resulting in high sticking probabilities and high cross-link densities in the resulting polymers. Figure 3 summarizes the dependence of the aggregation and redispersion rates on the dithiol-to-NC ratio.

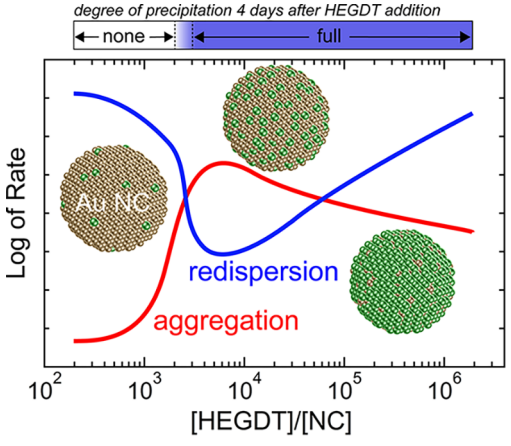

Figure 3. Schematic dependence of the rates of NC aggregation and redispersion on [HEGDT]/[NC]. Trends are deduced from extinction spectra. At both small and large ratios, aggregation is slow and redispersion is fast because the NCs have either a small coverage of linkers (at small ratios) or empty binding sites (at large ratios) and can form only a low density of cross-links. In contrast, aggregation is fast and redispersion is slow at intermediate ratios where more equal coverages of HEGDT and bare gold surface atoms promote a high cross-link density. Insets are models of three Au NCs with increasing HEGDT coverage (represented by green spheres) at higher values of [HEGDT]/[NC]. The blue color bar above the graph shows the degree of NC precipitation versus [HEGDT]/[NC] 4 days after HEGDT addition.

In addition to [HEGDT]/[NC], we found that the solution temperature also plays an important role in the kinetics of NC aggregation. We observed faster aggregation and precipitation at higher solution temperatures. For example, using [HEGDT]/[NC] = 4000, precipitation required 12 h at 8 °C but only a few minutes at 80 °C. Since the NC diffusivity increases by only 26% over this temperature range ($D \propto T$), such strong thermal activation indicates that the NC aggregation is a reaction-limited rather than diffusion-limited process. In contrast, changing the temperature had no effect on the rate of NC redispersion, suggesting that ozonation and redispersion are effectively activationless processes.

We tested the repeatability of the aggregation−redispersion cycle by consecutively adding dithiol and ozone to samples at [HEGDT]/[NC] = 4000 and room temperature. Figure 4a shows the postredispersion extinction spectra of a sample subjected to five cycles of precipitation and redispersion. The spectra at zero and one redispersion cycle are very similar to one another (see also Figure 1c). However, additional aggregation−redispersion cycles result in progressive weakening and broadening of the plasmonic peak to low energy, indicating increasingly incomplete redispersion after each cycle. TEM images reveal that these spectral changes are caused by fused NCs (Figure 4c), the number and size of which increase after each cycle. Most NC fusion probably occurs in the instant that ozone strips HEGDT from the precipitate and creates bare gold surfaces that then touch. Eventually, NC fusion becomes sufficiently extensive to prevent redispersion of a macroscopic fraction of the precipitate. We noticed some precipitate remaining at the bottom of the vial starting after the third redispersion (Figure 4d). The repeatability of this process may be better at other conditions (e.g., high [HEGDT]/[NC], which yields precipitates that redisperse much more quickly and therefore may provide less time for NC fusion to occur), but NC fusion may be difficult to completely avoid in these dense NC polymers.

Mass spectrometry, NMR spectroscopy, and pH measurements were used to determine the products of HEGDT ozonation in pure water (without NCs). Because ozone is a strong oxidant ($E°$ = 2.076 V in acidic solution), it can rapidly oxidize the thiol end groups of HEGDT to sulfonic acid (RSO_3H) and cleave the HEGDT backbone,[102,103] eventually mineralizing the molecule to CO_2, H_2O, and H_2SO_4. Indeed, electrospray ionization mass spectra of aqueous solutions of HEGDT showed quantitative conversion of HEGDT to a mixture of hexa(ethylene glycol) disulfonic acid (HEGDS) and various hydroxy and aldehyde sulfonic acid cleavage products after 5 min of ozonation (Figure S9). Of the common thiol oxidation intermediates, disulfinic acid (RSO_2H) and cyclic disulfide (RSSR), thiosulfinate (RS(O)SR), sulfinyl sulfone ($RSO_2S(O)R$), and α-disulfone (RSO_2SO_2R) were not observed, while we were unable to rule out the presence of disulfenic acid (RSOH) and cyclic α-disulfoxide (RS(O)S-(O)R), thiosulfonate (RSO_2SR), and sulfonic anhydride ($(RSO_2)_2O$) due to mass interferences with the HEGDS cleavage products. ^{1}H NMR spectra confirmed quantitative oxidation of the thiol groups of HEGDT to sulfonates within the first 5 min of ozonation (Figure 5a). Furthermore, we found that the pH of the ozonated solutions rapidly decreases to the value expected if each thiol group produces 1 equiv of a strong acid (Figure S10). Since sulfonic acids ($pK_a < 0$)[104] and sulfuric acid are the only thiol oxidation products that are strong acids in water, we can conclude from the pH, NMR, and

DOI: 10.1021/acs.jpcc.9b06976
J. Phys. Chem. C XXXX, XXX, XXX−XXX

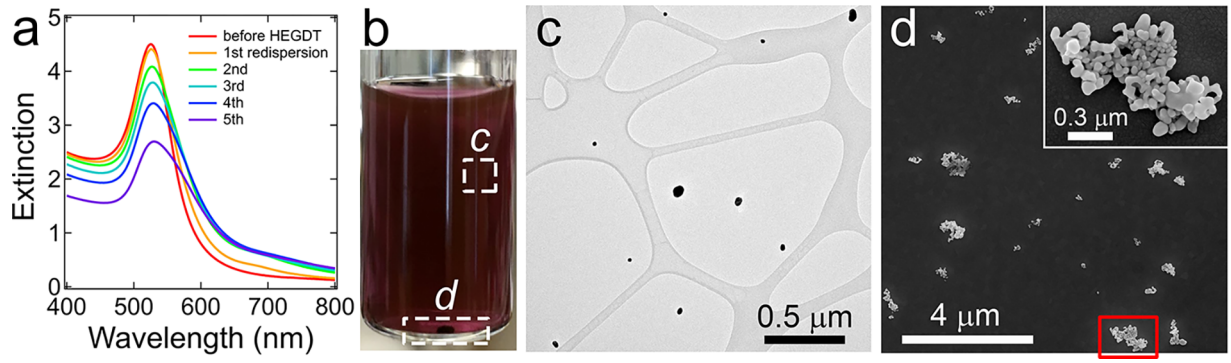

Figure 4. Repeatability of the NC precipitation−redispersion process. (a) Extinction spectra of a sample subjected to five cycles of HEGDT-induced precipitation ([HEGDT]/[NC] = 4000) and ozone-induced redispersion. Each spectrum was taken 7 days after ozonation to enable direct comparison with Figure 1. (b) Photograph of the sample after the fifth redispersion. The dispersion is purple-red and noticeably hazy. Note the residual precipitate at the bottom of the vial. (c) TEM image of a dried aliquot of the dispersion (taken from region c in panel b). (d) Scanning electron microscope image of the precipitate (from region d in panel b) deposited on a silicon wafer. The inset shows a heavily fused NC aggregate outlined in the small red box.

mass spectrometry data that ozonation of free HEGDT in solution produces a mixture of HEGDS, various hydroxy and aldehyde sulfonic acid fragments, and a small amount of H_2SO_4 (see below). We expect ozonation of HEGDT bound to the Au NCs to yield similar products. Our FTIR spectra prove that ozonation completely removes HEGDT from the NC precipitates (Figure S7), which is possible only if the thiolate anchoring groups are oxidized and stripped from the NC surface. Removal of surface sulfur was confirmed by X-ray photoelectron spectroscopy (Figure S11).

Quantitative NMR data were acquired to better understand the kinetics of HEGDT ozonation in pure D_2O. In general, the rate of this reaction will depend on the concentrations of both HEGDT and ozone. However, since $[O_3]$ is constant during bubbling in our process (Figure S12), the reaction is expected to exhibit pseudo-first-order kinetics with respect to [HEGDT]. Rather than quantifying [HEGDT] itself, which is difficult from 1D NMR data due to the presence of two identical terminal thiols per molecule, we used the protons of the methylene groups α to the thiols (labeled a in Figure 5a) to monitor the total thiol concentration. Time traces show that the thiol concentration decreases exponentially during ozonation following first-order kinetics with a thiol half-life of ∼50 s (Figure 5b,c). With this half-life, 98.5% of the thiol groups are oxidized in the first 5 min of ozonation. The sulfonate concentration (quantified with the α-methylene protons labeled a′ in Figure 5a) increases as the thiol concentration decreases. The sulfonate concentration peaks at 4−5 min and slowly declines thereafter as ozone cleaves the HEGDT backbone and releases sulfate ion. Qualitative analysis with barium chloride confirmed the presence of free sulfate after ozonation. Meanwhile, the concentration of ether groups in the oligo(ethylene glycol) backbone (protons c−f + c′−f′) also slowly decreases as the molecules are digested by ozone. We found that ∼15% of the ether methylene groups are destroyed during the first 5 min of ozonation, suggesting a significant amount of HEGDT fragmentation, in agreement with the mass spectrometry results discussed above. Moreover, a steady accumulation of formic acid (Figure 5b,c) indicates that some of the organic HEGDT fragments are rapidly oxidized. These ozonation studies were carried out on free molecules in D_2O. The kinetics should be faster in H_2O than D_2O. On the other hand, HEGDT ligands within the NC aggregates are likely to react more slowly due to steric crowding, so the reported thiol half-life may be considered a lower limit for the oxidation of the thiolate linkers that hold the NC polymer together.

Since sulfonates bind much less strongly than thiols to gold,[106,107] ozonation causes the NC polymer to lose its cross-linking and fall apart, but redispersion of the resulting NC monomers and oligomers depends strongly on the presence of ions in the solution that promote colloidal stability. We presumed that citrate ions are the main peptizing agents in the original NC reaction mixture and that NC redispersion into the reaction solution is facilitated by the citrate that survives ozonation. NMR data show that nearly all (∼97%) of the free citrate initially present in solution survives the 5 min ozone treatment and so is available to promote redispersion (Figure S13). To determine the role of citrate and the other major species in the reaction mixture, we tested redispersion as a function of solution composition by thoroughly rinsing batches of NC precipitates (made at [HEGDT]/[NC] = 4000) with water, then adding a supernatant of known composition and bubbling ozone in the normal way. The results are summarized in Table 1. In pure water, the NC precipitates completely dissolve but incompletely redisperse to form stable, deep blue colloids of NC agglomerates. Redispersion is improved by adding trisodium citrate to the supernatant. The sol color changes from blue to purple and then red as the citrate concentration is increased from 0.02 to 2.65 mM, indicating progressively more complete redispersion of the colloidal NCs. However, significant NC agglomerates persist even in 2.65 mM citrate (the citrate concentration of the original NC reaction mixture). We found that adding 1−10 mM of sodium chloride (NaCl) to the citrate solution causes nearly complete redispersion of the NCs, with extinction spectra very similar to those in the full reaction mixture (Figure 1c). Since adding NaCl without citrate had no effect on NC redispersion (see Table 1), we believe that coadsorption of citrate and chloride enhances inter-NC electrostatic repulsion and helps break up the colloidal NC agglomerates into individual charge-stabilized NCs. Of course, adding too much salt will decrease the Debye screening length enough to trigger NC flocculation. The same is true of citrate. As shown in Table 1, the NCs do not redisperse at all when the citrate concentration is too high (20 mM). Interestingly, no redispersion occurred in mM solutions

DOI: 10.1021/acs.jpcc.9b06976
J. Phys. Chem. C XXXX, XXX, XXX−XXX

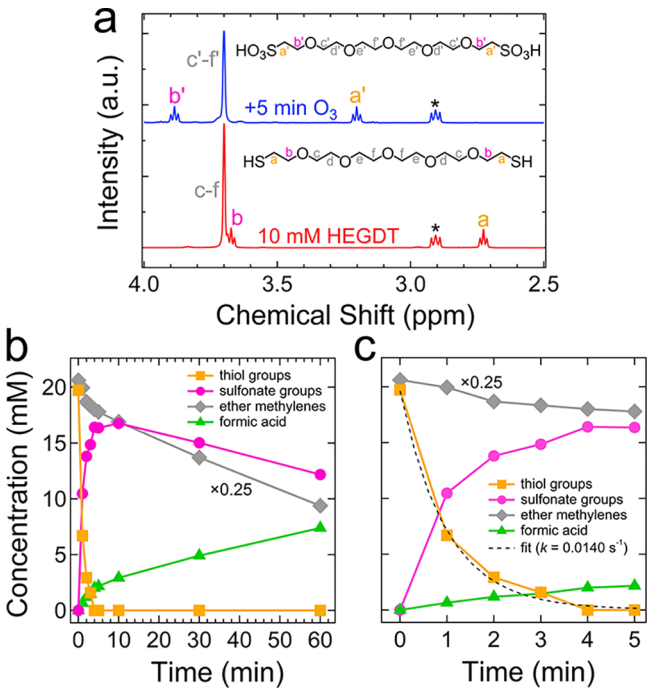

Figure 5. NMR analysis of the HEGDT ozonation products. (a) ^{1}H NMR spectra of a 10 mM solution of HEGDT in pure D_2O before and after 5 min of ozonation. The HEGDT spectrum shows the expected α-methylene triplet at 2.73 ppm (labeled a), β-methylene triplet at 3.67 ppm (labeled b), and oligo ethylene glycol backbone at 3.70 ppm (labeled c–f), in agreement with the literature.[105] After ozonation, the α- and β-methylene triplets shift downfield while the ether backbone peak area decreases by ∼15%. The postozonation spectrum is assigned to a mixture of hexa(ethylene glycol) disulfonic acid (HEGDS) and its breakdown products. The two triplets are assigned to the α- and β-methylene groups of sulfonate, while the backbone protons of HEGDS and its cleavage products are convolved in the large peak at 3.69 ppm. Labeled molecular structures of HEGDT and HEGDS are inset with each spectrum. Asterisks denote peaks from the internal standard. (b) Time traces of the concentrations of thiol groups (a protons), sulfonate groups (a′ protons), ether methylene groups (c–f and c′–f′ protons), and formic acid (quantified from the singlet peak observed at 8.22 ppm) during ozonation of the HEGDT solution. Note that the ether methylene data are multiplied by 0.25 for ease of plotting. (c) A magnified view of the data for the first 5 min of the reaction. The dashed line is an exponential fit to the thiol trace, with an extracted first-order rate constant of 0.0140 s^{-1}, giving a thiol half-life of ∼50 s.

of HEGDS (made by ozonation of aqueous HEGDT and adjusted to pH 6), probably because HEGDS has some affinity for binding to gold and can weakly cross-link the NCs when present at high concentrations in the absence of better ligands (such as citrate). We note that adding acetone (the other major component of the reaction solution, at 0.29 mM) had no effect on redispersion. These results show that upon ozonation, the depolymerized NCs spontaneously form colloidal NC agglomerates, even in pure water, but adsorption of citrate and chloride ions provides the extra electrostatic driving force needed to completely dissociate the agglomerates and form a sol of individual NCs.

Our NC precipitation–redispersion process is not limited to the use of HEGDT cross-linkers. Other multidentate thiols with sufficient water solubility are also effective, including 2,2′-(ethylenedioxy)diethanethiol, pentaerythritol tetrakis(3-mercaptopropionate), and 1,6-hexanedithiol (Figure S14).

Table 1. Effect of Solution Composition on NC Redispersion[a]

supernatant composition (mM)					
Na_3Cit	NaCl	HEGDS[b]	percentage of precipitate dissolved (%)	solution color	completeness of redispersion (%)[c]
0	*0*	*0*	*100*	*blue*	*50*
0.02	*0*	*0*	*100*	*blue*	*50*
0.2	0	0	100	purple	60
2	0	0	100	pink	70
2.65	0	0	100	red	80
20	0	0	0	colorless	0
0	*4.19*	*0*	*100*	*blue*	*50*
2.65	4.19	0	100	red	95
0	*0*	*0.1*	*100*	*blue*	*50*
0	0	0.5	20	gray	20
0	0	>1	0	colorless	0

[a]Italicized rows denote experiments with results indistinguishable from NC redispersion into pure water. [b]HEGDS = ozonated solutions of HEGDT adjusted to pH = 6 with NaOH. [c]Referenced to NC redispersion into the normal supernatant (the NC reaction mixture).

However, we found the concentration of dithiols with poor water solubility, such as biphenyl-4,4′-dithiol, is too low to trigger NC precipitation within a reasonable time (<weeks). While NC polymerization in water is facilitated by using water-soluble linkers, ozone-induced depolymerization is likely effective for all thiol linkers, regardless of their water solubility before ozonation.

Lastly, we briefly evaluated an alternative, ozone-free approach to depolymerizing dithiolate-linked Au NCs by exchanging the bound dithiols with monothiols. We reasoned that the NC polymers can be unzipped simply by displacing adsorbed HEGDT with a large excess of an appropriate monothiol.[108] The monothiols tested were hexa(ethylene glycol) monothiol (HEGMT) and 3-mercaptopropionic acid (MPA), both of which are soluble in water, as well as 11-mercaptoundecanoic acid (MUDA) and 16-mercapto-hexadecanoic acid (MHDA), which are poorly soluble in water and so were added as 0.1 M solutions in ethanol, resulting in the formation of micellar emulsions (see Methods). We first established that these monothiols cause no NC aggregation when added to the NC reaction mixture and are thus suitable ligands for dispersing the NCs. NC precipitates made at [HEGDT]/[NC] = 4000 were then incubated in the normal supernatant spiked with one of the monothiols at monothiol-to-NC ratios as large as 4×10^6. Partial redispersion was achieved using high concentrations of HEGMT ([HEGMT]/[NC] = 4×10^6), which completely dissolved the NC precipitates to form a pink sol after 6 days of incubation at room temperature (Figure S15). More aggressive exchange conditions (12 h of sonication at 75 °C in the presence of HEGMT) yielded red colloids consisting predominantly of individual NCs, but some of the NCs reprecipitated during these relatively harsh experiments (Figure S15). In contrast, the NCs showed no tendency to redisperse in aqueous MPA (pH 6) at either set of conditions, perhaps because van der Waals attraction between the MPA-capped NCs prevents the NC precipitates from dissolving. While MPA failed to redisperse the NCs, the longer-chain thiol acids MUDA and MHDA dissolved the NC precipitates to give pink-white emulsions that, upon filtering to remove the

DOI: 10.1021/acs.jpcc.9b06976
J. Phys. Chem. C XXXX, XXX, XXX–XXX

micelles, produced pink dispersions (after room-temperature aging) or red dispersions (after high-temperature sonication). Sonication in MUDA gave the most complete NC redispersion of any of the monothiol treatments (Figure S15), nearly comparable to the results obtained with ozonation. Overall, our experiments show that monothiol-mediated NC redispersion is promising, but ozonation is a simpler, cleaner, and more effective method for completely reversing the assembly of covalently cross-linked Au NC polymers.

CONCLUSIONS

We have shown that Au NCs covalently cross-linked by dithiols can be completely depolymerized and redispersed as stable hydrosols of individual NCs by brief treatment with ozone. Ozone quantitatively oxidizes the strongly bound dithiolate groups to weakly bound sulfonates and cleaves a fraction of the linkers into molecular fragments, thereby destroying the cross-linking and freeing the NCs to redisperse as charge-stabilized colloids. The speed of NC aggregation and redispersion depends on the dithiol concentration: at both low and high concentrations, aggregation is slow and redispersion is fast because the NCs have a small coverage of linkers or empty binding sites and can form only a low cross-link density, while at intermediate concentrations aggregation is fast and redispersion is slow because similar coverages of HEGDT and bare gold surface atoms enable a high sticking probability and cross-link density. Complete redispersion of the NCs is possible when the concentration of the peptizing agents (citrate and chloride in this case) is sufficiently high. The precipitation−redispersion cycle works with water-soluble thiol linkers and can be repeated multiple times, albeit with some irreversible fusion of NCs after each cycle. Redispersion of NCs by exchange of dithiols with monothiols was also demonstrated, but this approach was less effective than ozonation for achieving complete NC redispersion. Selective linker oxidation by ozone is a general way to reverse the aggregation of covalently linked Au NCs. Interesting future directions include using smaller, more controlled ozone doses to stop rather than reverse the aggregation of Au NCs and extending this approach to Ag NCs, which may require a milder oxidant than ozone.

ASSOCIATED CONTENT

Supporting Information

The Supporting Information is available free of charge on the ACS Publications website at DOI: 10.1021/acs.jpcc.9b06976.

Raman spectra, TEM images, optical extinction spectra, ozone quantification, fungal growth, FTIR evaluation of ligand exchange, mass spectrometry data, pH measurements, and evaluation of alternative linkers and monothiol-induced redispersion (PDF)

AUTHOR INFORMATION

Corresponding Author

*E-mail: lawm@uci.edu.

ORCID

Matt Law: 0000-0001-7645-9908

Notes

The authors declare no competing financial interest.

ACKNOWLEDGMENTS

This work was supported by the National Science Foundation Center for Chemical Innovation on Chemistry at the Space-Time Limit (CaSTL), Grant CHE-1414466. Materials characterization was performed at the user facilities of the UC Irvine Materials Research Institute (IMRI), including instrumentation funded in part by the National Science Foundation Major Research Instrumentation Program under Grant CHE-1338173. We thank the UCI Laser Spectroscopy Labs for use of the Raman spectrometer. This research used resources of the Advanced Light Source, which is a DOE Office of Science User Facility under Contract DE-AC02-05CH11231. We thank Ara Apkarian and Christian Engelbrekt for helpful discussions.

REFERENCES

(1) Brust, M.; Walker, M.; Bethell, D.; Schiffrin, D. J.; Whyman, R. Synthesis of thiol-derivatised gold nanoparticles in a two-phase liquid-liquid system. *J. Chem. Soc., Chem. Commun.* **1994**, 801−802.

(2) Daniel, M.-C.; Astruc, D. Gold nanoparticles: Assembly, supramolecular chemistry, quantum-size-related properties, and applications toward biology, catalysis, and nanotechnology. *Chem. Rev.* **2004**, *104*, 293−346.

(3) Romo-Herrera, J. M.; Alvarez-Puebla, R. A.; Liz-Marzán, L. M. Controlled assembly of plasmonic nanoparticle clusters. *Nanoscale* **2011**, *3*, 1304−1315.

(4) Grzelczak, M.; Liz-Marzán, L. M. Colloidal nanoplasmonics: From building blocks to sensing devices. *Langmuir* **2013**, *29*, 4652−4663.

(5) Klinkova, A.; Choueiri, R. M.; Kumacheva, E. Self-assembled plasmonic nanostructures. *Chem. Soc. Rev.* **2014**, *43*, 3976−3991.

(6) Hill, L. J.; Pinna, N.; Char, K.; Pyun, J. Colloidal polymers from inorganic nanoparticle monomers. *Prog. Polym. Sci.* **2015**, *40*, 85−120.

(7) Qian, Z.; Ginger, D. S. Reversibly reconfigurable colloidal plasmonic nanomaterials. *J. Am. Chem. Soc.* **2017**, *139*, 5266−5276.

(8) Yang, W.-H.; Schatz, G. C.; Van Duyne, R. P. Discrete dipole approximation for calculating extinction and Raman intensities for small particles with arbitrary shapes. *J. Chem. Phys.* **1995**, *103*, 869−875.

(9) Elghanian, R.; Storhoff, J. J.; Mucic, R. C.; Letsinger, R. L.; Mirkin, C. A. Selective colorimetric detection of polynucleotides based on the distance-dependent optical properties of gold nanoparticles. *Science* **1997**, *277*, 1078−1081.

(10) Tang, L.; Li, J. Plasmon-based colorimetric nanosensors for ultrasensitive molecular diagnostics. *ACS Sens.* **2017**, *2*, 857−875.

(11) Gilroy, K. D.; Xia, Y. Dimerization of colloidal particles through controlled aggregation for enhanced properties and applications. *Chem. - Asian J.* **2016**, *11*, 2341−2351.

(12) Mirkin, C. A.; Letsinger, R. L.; Mucic, R. C.; Storhoff, J. J. A DNA-based method for rationally assembling nanoparticles into macroscopic materials. *Nature* **1996**, *382*, 607−609.

(13) Dujardin, E.; Hsin, L.-B.; Wang, C. R. C.; Mann, S. DNA-driven self-assembly of gold nanorods. *Chem. Commun.* **2001**, 1264−1265.

(14) Liu, J.; Lu, Y. Fast colorimetric sensing of adenosine and cocaine based on a general sensor design involving aptamers and nanoparticles. *Angew. Chem., Int. Ed.* **2006**, *45*, 90−94.

(15) Lee, S. E.; Chen, Q.; Bhat, R.; Petkiewicz, S.; Smith, J. M.; Ferry, V. E.; Correia, A. L.; Alivisatos, A. P.; Bissell, M. J. Reversible aptamer-Au plasmon rulers for secreted single molecules. *Nano Lett.* **2015**, *15*, 4564−4570.

(16) Shenton, W.; Davis, S. A.; Mann, S. Directed self-assembly of nanoparticles into macroscopic materials using antibody-antigen recognition. *Adv. Mater.* **1999**, *11*, 449−452.

(17) Sastry, M.; Lala, N.; Patil, V.; Chavan, S. P.; Chittiboyina, A. G. Optical absorption study of the biotin-avidin interaction on colloidal silver and gold particles. *Langmuir* **1998**, *14*, 4138−4142.

DOI: 10.1021/acs.jpcc.9b06976
J. Phys. Chem. C XXXX, XXX, XXX−XXX

(18) Connolly, S.; Fitzmaurice, D. Programmed assembly of gold nanocrystals in aqueous solution. *Adv. Mater.* **1999**, *11*, 1202−1205.
(19) Lévy, R.; Thanh, N. T. K.; Doty, R. C.; Hussain, I.; Nichols, R. J.; Schiffrin, D. J.; Brust, M.; Fernig, D. G. Rational and combinatorial design of peptide capping ligands for gold nanoparticles. *J. Am. Chem. Soc.* **2004**, *126*, 10076−10084.
(20) Si, S.; Mandal, T. K. pH-controlled reversible assembly of peptide-functionalized gold nanoparticles. *Langmuir* **2007**, *23*, 190−195.
(21) Raula, J.; Shan, J.; Nuopponen, M.; Niskanen, A.; Jiang, H.; Kauppinen, E. I.; Tenhu, H. Synthesis of gold nanoparticles grafted with a thermoresponsive polymer by surface-induced reversible-addition-fragmentation chain-transfer polymerization. *Langmuir* **2003**, *19*, 3499−3504.
(22) Zhu, M.-Q.; Wang, L.-Q.; Exarhos, G. J.; Li, A. D. Q. Thermosensitive gold nanoparticles. *J. Am. Chem. Soc.* **2004**, *126*, 2656−2657.
(23) Fava, D.; Winnik, M. A.; Kumacheva, E. Photothermally-triggered self-assembly of gold nanorods. *Chem. Commun.* **2009**, 2571−2573.
(24) Ding, T.; Valev, V. K.; Salmon, A. R.; Forman, C. J.; Smoukov, S. K.; Scherman, O. A.; Frenkel, D.; Baumberg, J. J. Light-induced actuating nanotransducers. *Proc. Natl. Acad. Sci. U. S. A.* **2016**, *113*, 5503−5507.
(25) Liu, K.; Nie, Z.; Zhao, N.; Li, W.; Rubinstein, M.; Kumacheva, E. Step-growth polymerization of inorganic nanoparticles. *Science* **2010**, *329*, 197−200.
(26) Sánchez-Iglesias, A.; Grzelczak, M.; Altantzis, T.; Goris, B.; Pérez-Juste, J.; Bals, S.; Van Tendeloo, G.; Donaldson, S. H., Jr.; Chmelka, B. F.; Israelachvili, J. N.; Liz-Marzán. Hydrophobic interactions modulate self-assembly of nanoparticles. *ACS Nano* **2012**, *6*, 11059−11065.
(27) Kitayama, Y.; Takeuchi, T. Synthesis of CO_2/N_2-triggered reversible stability-controllable poly(2-(diethylamino)ethyl methacrylate)-grafted-AuNPs by surface-initiated atom transfer radical polymerization. *Langmuir* **2014**, *30*, 12684−12689.
(28) Fullam, S.; Rao, S. N.; Fitzmaurice, D. Noncovalent self-assembly of silver nanocrystal aggregates in solution. *J. Phys. Chem. B* **2000**, *104*, 6164−6173.
(29) Boal, A. K.; Ilhan, F.; DeRouchey, J. E.; Thurn-Albrecht, T.; Russell, T. P.; Rotello, V. M. Self-assembly of nanoparticles into structured spherical and network aggregates. *Nature* **2000**, *404*, 746−748.
(30) Mandal, S.; Gole, A.; Lala, N.; Gonnade, R.; Ganvir, V.; Sastry, M. Studies on the reversible aggregation of cysteine-capped colloidal silver particles interconnected via hydrogen bonds. *Langmuir* **2001**, *17*, 6262−6268.
(31) Templeton, A. C.; Zamborini, F. P.; Wuelfing, W. P.; Murray, R. W. Controlled and reversible formation of nanoparticle aggregates and films using Cu^{2+}-carboxylate chemistry. *Langmuir* **2000**, *16*, 6682−6688.
(32) Kim, Y.; Johnson, R. C.; Hupp, J. T. Gold nanoparticle-based sensing of "spectroscopically silent" heavy metal ions. *Nano Lett.* **2001**, *1*, 165−167.
(33) Liu, J.; Mendoza, S.; Román, E.; Lynn, M. J.; Xu, R.; Kaifer, A. E. Cyclodextrin-modified gold nanospheres. Host-guest interactions at work to control colloidal properties. *J. Am. Chem. Soc.* **1999**, *121*, 4304−4305.
(34) Olson, M. A.; Coskun, A.; Klajn, R.; Fang, L.; Dey, S. K.; Browne, K. P.; Grzybowski, B. A.; Stoddart, J. F. Assembly of polygonal nanoparticle clusters directed by reversible noncovalent bonding interactions. *Nano Lett.* **2009**, *9*, 3185−3190.
(35) Naka, K.; Itoh, H.; Chujo, Y. Temperature-dependent reversible self-assembly of gold nanoparticles into spherical aggregates by molecular recognition between pyrenyl and dinitrophenyl units. *Langmuir* **2003**, *19*, 5496−5501.
(36) Han, X.; Goebl, J.; Lu, Z.; Yin, Y. Role of salt in the spontaneous assembly of charged gold nanoparticles in ethanol. *Langmuir* **2011**, *27*, 5282−5289.
(37) Liu, Y.; Han, X.; He, L.; Yin, Y. Thermoresponsive assembly of charged gold nanoparticles and their reversible tuning of plasmon coupling. *Angew. Chem., Int. Ed.* **2012**, *51*, 6373−6377.
(38) Sidhaye, D. S.; Kashyap, S.; Sastry, M.; Hotha, S.; Prasad, B. L. V. Gold nanoparticle networks with photoresponsive interparticle spacings. *Langmuir* **2005**, *21*, 7979−7984.
(39) Klajn, R.; Bishop, K. J. M.; Grzybowski, B. A. Light-controlled self-assembly of reversible and irreversible nanoparticle supra-structures. *Proc. Natl. Acad. Sci. U. S. A.* **2007**, *104*, 10305−10309.
(40) Wei, Y.; Han, S.; Kim, J.; Soh, S.; Grzybowski, B. A. Photoswitchable catalysis mediated by dynamic aggregation of nanoparticles. *J. Am. Chem. Soc.* **2010**, *132*, 11018−11020.
(41) Kim, T.; Lee, K.; Gong, M.-S.; Joo, S.-W. Control of gold nanoparticle aggregates by manipulation of interparticle interaction. *Langmuir* **2005**, *21*, 9524−9528.
(42) Maye, M. M.; Lim, I.-I. S.; Luo, J.; Rab, J.; Rabinovich, D.; Liu, T.; Zhong, C.-J. Mediator-template assembly of nanoparticles. *J. Am. Chem. Soc.* **2005**, *127*, 1519−1529.
(43) Lin, L.; Peng, X.; Wang, M.; Scarabelli, L.; Mao, Z.; Liz-Marzán, L. M.; Becker, M. F.; Zheng, Y. Light-directed reversible assembly of plasmonic nanoparticles using plasmon-enhanced thermophoresis. *ACS Nano* **2016**, *10*, 9659−9668.
(44) Patra, P. P.; Chikkaraddy, R.; Tripathi, R. P. N.; Dasgupta, A.; Kumar, G. V. P. Plasmofluidic single-molecule surface-enhanced Raman scattering from dynamic assembly of plasmonic nanoparticles. *Nat. Commun.* **2014**, *5*, 4357.
(45) He, H.; Feng, M.; Chen, Q.; Zhang, X.; Zhan, H. Light-induced reversible self-assembly of gold nanoparticles surface-immobilized with coumarin ligands. *Angew. Chem., Int. Ed.* **2016**, *55*, 936−940.
(46) Guarise, C.; Pasquato, L.; Scrimin, P. Reversible aggregation/deaggregation of gold nanoparticles induced by a cleavable dithiol linker. *Langmuir* **2005**, *21*, 5537−5541.
(47) Lim, I.-I. S.; Vaiana, C.; Zhang, Z.-Y.; Zhang, Y.-J.; An, D.-L.; Zhong, C.-J. X-shaped rigid arylethynes to mediate the assembly of nanoparticles. *J. Am. Chem. Soc.* **2007**, *129*, 5368−5369.
(48) Sung, K.-M.; Mosley, D. W.; Peelle, B. R.; Zhang, S.; Jacobson, J. M. Synthesis of monofunctionalized gold nanoparticles by Fmoc solid-phase reactions. *J. Am. Chem. Soc.* **2004**, *126*, 5064−5065.
(49) Xu, X.; Rosi, N. L.; Wang, Y.; Huo, F.; Mirkin, C. A. Asymmetric functionalization of gold nanoparticles with oligonucleotides. *J. Am. Chem. Soc.* **2006**, *128*, 9286−9287.
(50) Sardar, R.; Heap, T. B.; Shumaker-Parry, J. S. Versatile solid phase synthesis of gold nanoparticle dimers using an asymmetric functionalization approach. *J. Am. Chem. Soc.* **2007**, *129*, 5356−5357.
(51) Rycenga, M.; McLellan, J. M.; Xia, Y. Controlling the assembly of silver nanocubes through selective functionalization of their faces. *Adv. Mater.* **2008**, *20*, 2416−2420.
(52) Maye, M. M.; Nykypanchuk, D.; Cuisinier, M.; van der Lelie, D.; Gang, O. Stepwise surface encoding for high-throughput assembly of nanoclusters. *Nat. Mater.* **2009**, *8*, 388−391.
(53) Gu, H.; Yang, Z.; Gao, J.; Chang, C. K.; Xu, B. Heterodimers of nanoparticles: Formation at a liquid-liquid interface and particle-specific surface modification by functional molecules. *J. Am. Chem. Soc.* **2005**, *127*, 34−35.
(54) Yim, T.-J.; Wang, Y.; Zhang, X. Synthesis of a gold nanoparticle dimer plasmonic resonator through two-phase-mediated functionalization. *Nanotechnology* **2008**, *19*, 435605.
(55) Cho, E. C.; Choi, S.-W.; Camargo, P. H. C.; Xia, Y. Thiol-induced assembly of Au nanoparticles into chainlike structures and their fixing by encapsulation in silica shells or gelatin microspheres. *Langmuir* **2010**, *26*, 10005−10012.
(56) Wang, X.; Li, G.; Chen, T.; Yang, M.; Zhang, Z.; Wu, T.; Chen, H. Polymer-encapsulated gold-nanoparticle dimers: Facile preparation and catalytical application in guided growth of dimeric ZnO-nanowires. *Nano Lett.* **2008**, *8*, 2643−2647.
(57) Chen, G.; Wang, Y.; Tan, L. H.; Yang, M.; Tan, L. S.; Chen, Y.; Chen, H. High-purity separation of gold nanoparticle dimers and trimers. *J. Am. Chem. Soc.* **2009**, *131*, 4218−4219.

DOI: 10.1021/acs.jpcc.9b06976
J. Phys. Chem. C XXXX, XXX, XXX−XXX

(58) Braun, G. B.; Lee, S. J.; Laurence, T.; Fera, N.; Fabris, L.; Bazan, G. C.; Moskovits, M.; Reich, N. O. Generalized approach to SERS-active nanomaterials via controlled nanoparticle linking, polymer encapsulation, and small-molecule infusion. *J. Phys. Chem. C* **2009**, *113*, 13622−13629.
(59) Nooney, R. I.; Thirunavukkarasu, D.; Chen, Y.; Josephs, R.; Ostafin, A. E. Self-assembly of mesoporous nanoscale silica/gold composites. *Langmuir* **2003**, *19*, 7628−7637.
(60) Brown, L. O.; Doorn, S. K. A controlled and reproducible pathway to dye-tagged, encapsulated silver nanoparticles as substrates for SERS multiplexing. *Langmuir* **2008**, *24*, 2277−2280.
(61) Stewart, A. F.; Lee, A.; Ahmed, A.; Ip, S.; Kumacheva, E.; Walker, G. C. Rational design for the controlled aggregation of gold nanorods via phospholipid encapsulation for enhanced Raman scattering. *ACS Nano* **2014**, *8*, 5462−5467.
(62) Alivisatos, A. P.; Johnsson, K. P.; Peng, X.; Wilson, T. E.; Loweth, C. J.; Bruchez, M. P., Jr.; Schultz, P. G. Organization of 'nanocrystal molecules' using DNA. *Nature* **1996**, *382*, 609−611.
(63) Lim, D.-K.; Jeon, K.-S.; Kim, H. M.; Nam, J.-M.; Suh, Y. D. Nanogap-engineerable Raman-active nanodumbbells for single-molecule detection. *Nat. Mater.* **2010**, *9*, 60−67.
(64) Caswell, K. K.; Wilson, J. N.; Bunz, U. H. F.; Murphy, C. J. Preferential end-to-end assembly of gold nanorods by biotin-streptavidin connectors. *J. Am. Chem. Soc.* **2003**, *125*, 13914−13915.
(65) DeVries, G. A.; Brunnbauer, M.; Hu, Y.; Jackson, A. M.; Long, B.; Neltner, B. T.; Uzun, O.; Wunsch, B. H.; Stellacci, F. Divalent metal nanoparticles. *Science* **2007**, *315*, 358−361.
(66) Krüger, C.; Agarwal, S.; Greiner, A. Stoichiometric functionalization of gold nanoparticles in solution through a free radical polymerization approach. *J. Am. Chem. Soc.* **2008**, *130*, 2710−2711.
(67) Brousseau, L. C., III; Novak, J. P.; Marinakos, S. M.; Feldheim, D. L. Assembly of phenylacetylene-bridged gold nanocluster dimers and trimers. *Adv. Mater.* **1999**, *11*, 447−449.
(68) Joseph, S. T. S.; Ipe, B. I.; Pramod, P.; Thomas, K. G. Gold nanorods to nanochains: Mechanistic investigations on their longitudinal assembly using α,ω-alkanedithiols and interplasmon coupling. *J. Phys. Chem. B* **2006**, *110*, 150−157.
(69) Fabris, L.; Dante, M.; Nguyen, T.-Q.; Tok, J. B.-H.; Bazan, G. C. SERS aptatags: New responsive metallic nanostructures for heterogeneous protein detection by surface enhanced Raman spectroscopy. *Adv. Funct. Mater.* **2008**, *18*, 2518−2525.
(70) Whitmore, D. D.; El-Khoury, P. Z.; Fabris, L.; Chu, P.; Bazan, G. C.; Potma, E. O.; Apkarian, V. A. High sensitivity surface-enhanced Raman scattering in solution using engineered silver nanosphere dimers. *J. Phys. Chem. C* **2011**, *115*, 15900−15907.
(71) Banik, M.; Nag, A.; El-Khoury, P. Z.; Rodriguez Perez, A.; Guarrotxena, N.; Bazan, G. C.; Apkarian, V. A. Surface-enhanced Raman scattering of a single nanodumbbell: Dibenzyldithiol-linked silver nanospheres. *J. Phys. Chem. C* **2012**, *116*, 10415−10423.
(72) Izquierdo-Lorenzo, I.; Kubackova, J.; Manchon, D.; Mosset, A.; Cottancin, E.; Sanchez-Cortes, S. Linking Ag nanoparticles by aliphatic α,ω-dithiols: A study of the aggregation and formation of interparticle hot spots. *J. Phys. Chem. C* **2013**, *117*, 16203−16212.
(73) Wang, Y.; Chen, G.; Yang, M.; Silber, G.; Xing, S.; Tan, L. H.; Wang, F.; Feng, Y.; Liu, X.; Li, S.; Chen, H. A systems approach towards the stoichiometry-controlled hetero-assembly of nanoparticles. *Nat. Commun.* **2010**, *1*, 87.
(74) Li, W.; Camargo, P. H. C.; Lu, X.; Xia, Y. Dimers of silver nanospheres: Facile synthesis and their use as hot spots for surface-enhanced Raman scattering. *Nano Lett.* **2009**, *9*, 485−490.
(75) Cheng, L.; Song, J.; Yin, J.; Duan, H. Self-assembled plasmonic dimers of amphiphilic gold nanocrystals. *J. Phys. Chem. Lett.* **2011**, *2*, 2258−2262.
(76) Wang, H.; Schaefer, K.; Moeller, M. In situ immobilization of gold nanoparticle dimers in silica nanoshell by microemulsion coalescence. *J. Phys. Chem. C* **2008**, *112*, 3175−3178.
(77) Nepal, D.; Park, K.; Vaia, R. A. High-yield assembly of soluble and stable gold nanorod pairs for high-temperature plasmonics. *Small* **2012**, *8*, 1013−1020.
(78) Fontana, J.; Charipar, N.; Flom, S. R.; Naciri, J.; Piqué, A.; Ratna, B. R. Rise of the charge transfer plasmon: Programmable concatenation of conductively linked gold nanorods dimers. *ACS Photonics* **2016**, *3*, 904−911.
(79) Novak, J. P.; Nickerson, C.; Franzen, S.; Feldheim, D. L. Purification of molecularly bridged metal nanoparticle arrays by centrifugation and size exclusion chromatography. *Anal. Chem.* **2001**, *73*, 5758−5761.
(80) Tyler, T. P.; Henry, A.-I.; Van Duyne, R. P.; Hersam, M. C. Improved monodispersity of plasmonic nanoantennas via centrifugal processing. *J. Phys. Chem. Lett.* **2011**, *2*, 218−222.
(81) Alexander, K. D.; Hampton, M. J.; Zhang, S.; Dhawan, A.; Xu, H.; Lopez, R. A high-throughput method for controlled hot-spot fabrication in SERS-active gold nanoparticle dimer arrays. *J. Raman Spectrosc.* **2009**, *40*, 2171−2175.
(82) Lee, S. Y.; Hung, L.; Lang, G. S.; Cornett, J. E.; Mayergoyz, I. D.; Rabin, O. Dispersion in the SERS enhancement with silver nanocube dimers. *ACS Nano* **2010**, *4*, 5763−5772.
(83) Osberg, K. D.; Rycenga, M.; Harris, N.; Schmucker, A. L.; Langille, M. R.; Schatz, G. C.; Mirkin, C. A. Dispersible gold nanorod dimers with sub-5 nm gaps as local amplifiers for surface-enhanced Raman scattering. *Nano Lett.* **2012**, *12*, 3828−3832.
(84) Brust, M.; Schiffrin, D. J.; Bethell, D.; Kiely, C. J. Novel gold-dithiol nano-networks with non-metallic electronic properties. *Adv. Mater.* **1995**, *7*, 795−797.
(85) Puckett, S. D.; Heuser, J. A.; Keith, J. D.; Spendel, W. U.; Pacey, G. E. Interaction of ozone with gold nanoparticles. *Talanta* **2005**, *66*, 1242−1246.
(86) Ershov, B. G.; Abkhalimov, E. V.; Roldughin, V. I.; Rudoy, V. M.; Dement'eva, O. V.; Solovov, R. D. Adsorption of ozone and plasmonic properties of gold hydrosol: the effect of the nanoparticle size. *Phys. Chem. Chem. Phys.* **2015**, *17*, 18431−18436.
(87) Morozov, P. A.; Ershov, B. G.; Abkhalimov, E. V.; Dement'eva, O. V.; Rumyantseva, T. B.; Rudoy, V. M.; Roldughin, V. I. Aggregation stability of gold citrate hydrosol: Effect of ozone. *Colloid J.* **2011**, *73*, 668−675.
(88) Elliott, E. W., III; Glover, R. D.; Hutchison, J. E. Removal of thiol ligands from surface-confined nanoparticles without particle growth or desorption. *ACS Nano* **2015**, *9*, 3050−3059.
(89) Puspitasari, I.; Skupien, E.; Kapteijn, F.; Kooyman, P. J. Au capping agent removal using plasma at mild temperature. *Catalysts* **2016**, *6*, 179.
(90) Bastús, N. G.; Comenge, J.; Puntes, V. Kinetically controlled seeded growth synthesis of citrate-stabilized gold nanoparticles of up to 200 nm: Size focusing versus Ostwald ripening. *Langmuir* **2011**, *27*, 11098−11105.
(91) Levanov, A. V.; Isaikina, O. Y.; Tyutyunnik, A. N.; Antipenko, E. E.; Lunin, V. V. Molar absorption coefficient of ozone in aqueous solutions. *J. Anal. Chem.* **2016**, *71*, 549−553.
(92) Ilavsky, J. Nika: software for two-dimensional data reduction. *J. Appl. Crystallogr.* **2012**, *45*, 324−328.
(93) Wuelfing, W. P.; Gross, S. M.; Miles, D. T.; Murray, R. W. Nanometer gold clusters protected by surface-bound monolayers of thiolated poly(ethylene glycol) polymer electrolyte. *J. Am. Chem. Soc.* **1998**, *120*, 12696−12697.
(94) Bartz, M.; Küther, J.; Nelles, G.; Weber, N.; Seshadri, R.; Tremel, W. Monothiols derived from glycols as agents for stabilizing gold colloids in water: Synthesis, self-assembly and use as crystallization templates. *J. Mater. Chem.* **1999**, *9*, 1121−1125.
(95) Foos, E. E.; Snow, A. W.; Twigg, M. E.; Ancona, M. G. Thiol-terminated di-, tri-, and tetraethylene oxide functionalized gold nanoparticles: A water-soluble, charge-neutral cluster. *Chem. Mater.* **2002**, *14*, 2401−2408.
(96) Kanaras, A. G.; Kamounah, F. S.; Schaumburg, K.; Kiely, C. J.; Brust, M. Thioalkylated tetraethylene glycol: A new ligand for water soluble monolayer protected gold clusters. *Chem. Commun.* **2002**, 2294−2295.

DOI: 10.1021/acs.jpcc.9b06976
J. Phys. Chem. C XXXX, XXX, XXX−XXX

(97) Li, G.; Wang, T.; Bhosale, S.; Zhang, Y.; Fuhrhop, J.-H. Completely reversible aggregation of nanoparticles by varying the pH. *Colloid Polym. Sci.* **2003**, *281*, 1099−1103.
(98) Matsumi, Y.; Kawasaki, M. Photolysis of atmospheric ozone in the ultraviolet region. *Chem. Rev.* **2003**, *103*, 4767−4782.
(99) Bigall, N. C.; Reitzig, M.; Naumann, W.; Simon, P.; van Pée, K.-H.; Eychmüller, A. Fungal templates for noble-metal nanoparticles and their application in catalysis. *Angew. Chem., Int. Ed.* **2008**, *47*, 7876−7879.
(100) Park, J.-W.; Shumaker-Parry, J. S. Strong resistance of citrate anions on metal nanoparticles to desorption under thiol functionalization. *ACS Nano* **2015**, *9*, 1665−1682.
(101) Park, J.-W.; Shumaker-Parry, J. S. Structural study of citrate layers on gold nanoparticles: role of intermolecular interactions in stabilizing nanoparticles. *J. Am. Chem. Soc.* **2014**, *136*, 1907−1921.
(102) Andreozzi, R.; Caprio, V.; Insola, A. Kinetics and mechanisms of polyethyleneglycol fragmentation by ozone in aqueous solution. *Water Res.* **1996**, *30*, 2955−2960.
(103) Suzuki, J. Study on ozone treatment of water-soluble polymers. I. Ozone degradation of polyethylene glycol in water. *J. Appl. Polym. Sci.* **1976**, *20*, 93−103.
(104) Oea, S.; Doi, J. T. *Organic Sulfur Chemistry: Structure and Mechanism*; CRC Press: Boca Raton, FL, 1991.
(105) Mulay, P.; Shrikhande, G.; Puskas, J. E. Synthesis of mono- and dithiols of tetraethylene glycol and poly(ethylene glycol)s via enzyme catalysis. *Catalysts* **2019**, *9*, 228.
(106) Garrell, R. L.; Chadwick, J. E.; Severance, D. L.; McDonald, N. A.; Myles, D. C. Adsorption of sulfur containing molecules on gold: The effect of oxidation on monolayer formation and stability characterized by experiments and theory. *J. Am. Chem. Soc.* **1995**, *117*, 11563−11571.
(107) Joseph, Y.; Guse, B.; Nelles, G. Aging of 1,ω-alkyldithiol interlinked Au nanoparticle networks. *Chem. Mater.* **2009**, *21*, 1670−1676.
(108) Hostetler, M. J.; Templeton, A. C.; Murray, R. W. Dynamics of place-exchange reactions on monolayer-protected gold cluster molecules. *Langmuir* **1999**, *15*, 3782−3789.

DOI: 10.1021/acs.jpcc.9b06976
J. Phys. Chem. C XXXX, XXX, XXX−XXX

Supporting Information

for

Reversible Aggregation of Covalently Cross-Linked Gold Nanocrystals by Linker Oxidation

Zhongyue Luan,[1] Trenton Salk,[2] Alex Abelson,[1] Stephanie Jean,[3] Matt Law[1,4]*

[1]Department of Materials Science & Engineering, University of California, Irvine, Irvine, CA 92697

[2]Department of Physics and Astronomy, University of California, Irvine, Irvine, CA 92697

[3]Department of Chemistry, College of Saint Benedict, St. Joseph, MN 56374

[4]Department of Chemistry, University of California, Irvine, Irvine, CA 92697

**e-mail: lawm@uci.edu*

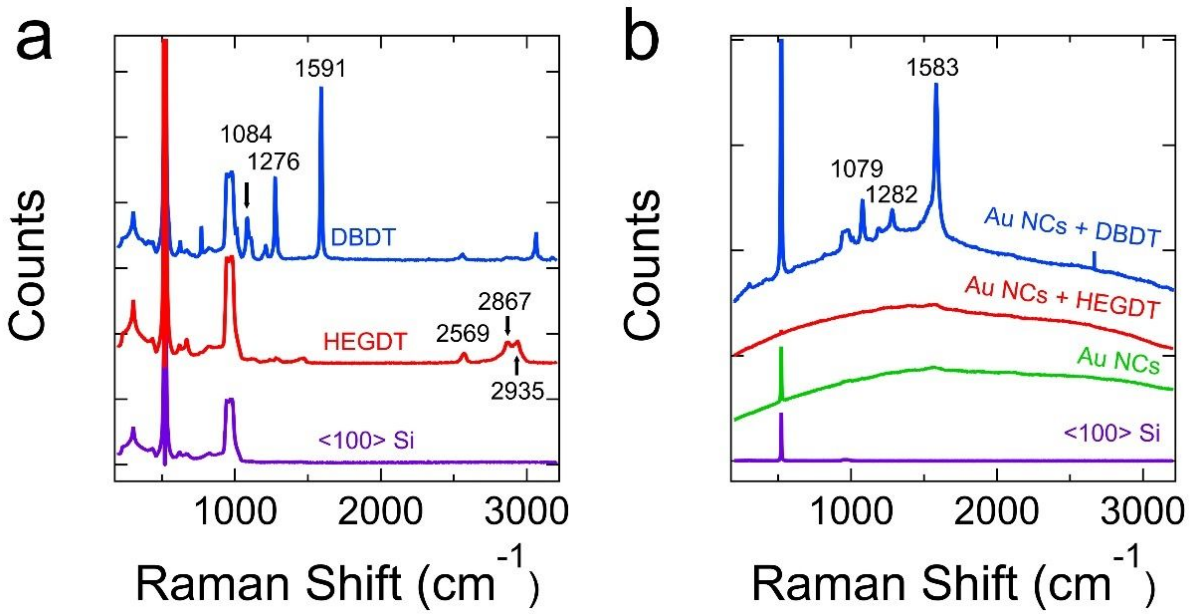

Figure S1. Comparison of Raman and surface-enhanced Raman spectra of HEGDT and biphenyl-4,4'-dithiol (DBDT). (a) Raman spectra a neat DBDT film (blue) and a HEGDT film (red) deposited on Si substrates. Several peaks are labeled. A spectrum of a clean Si substrate is included for reference. (b) Raman spectra of Au NC aggregates made with DBDT in THF (blue) and HEGDT in water (red) deposited on Si substrates. DBDT peaks are labeled. Reference spectra of untreated Au NCs (green) and a clean Si substrate are also included.

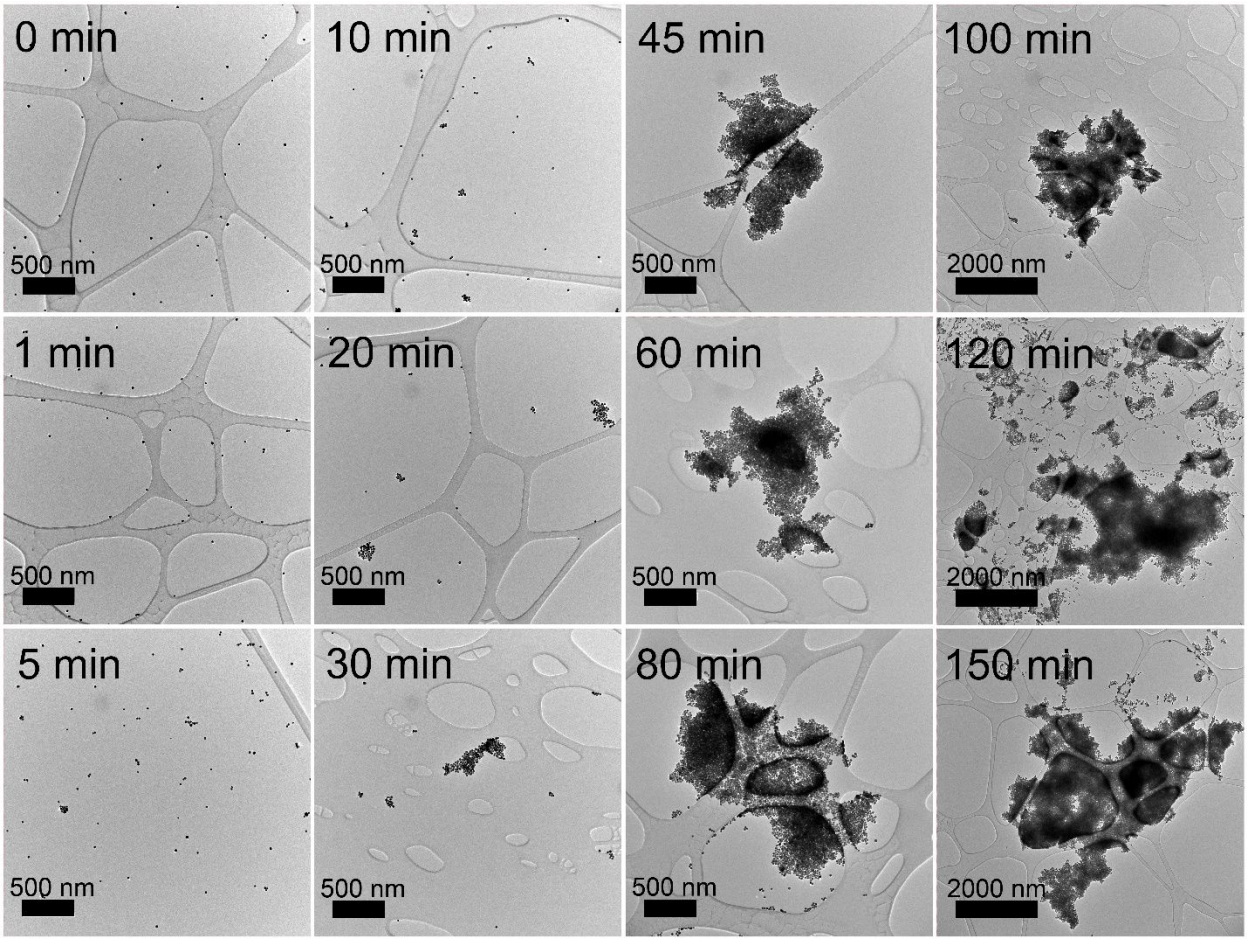

Figure S2. A time series of TEM images showing the aggregation process of Au NCs upon addition of HEGDT. Labels indicate the time after HEGDT addition (0 min refers to the as-made NC colloid without HEGDT). The samples were prepared using a technique that minimizes the artificial formation of NC aggregates during drying of the solution on the TEM grid (see Methods).

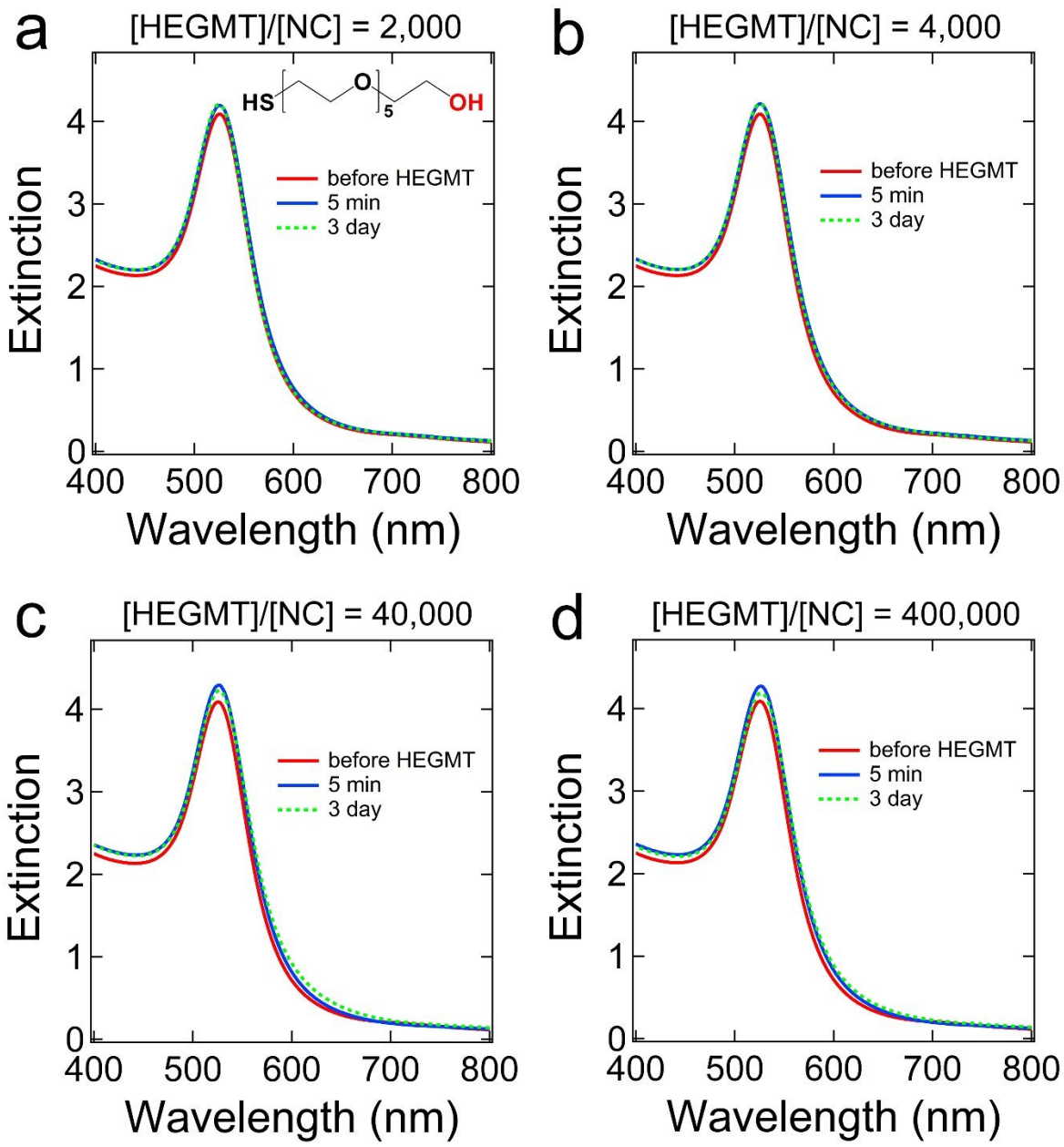

Figure S3. Optical extinction spectra of Au NC dispersions before and after adding four different concentrations of hexa(ethylene glycol) monothiol (HEGMT). (a) [HEGMT]/[NC] = 2,000. The structure of HEGMT is shown as an inset. (b) [HEGMT]/[NC] = 4,000. (c) [HEGMT]/[NC] = 40,000. (d) [HEGMT]/[NC] = 400,000. The NCs remain dispersed and show no aggregation even after three days of storage at ambient laboratory conditions.

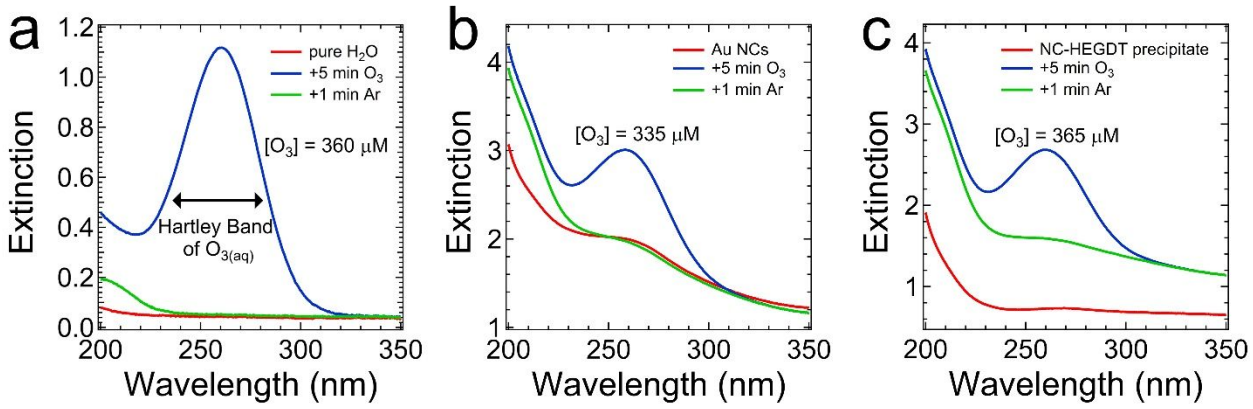

Figure S4. UV optical extinction spectra (200-350 nm) of (a) ultrapure water, (b) Au NCs, and (c) NC-HEGDT precipitates before adding ozone (red curves), immediately after 5 min of ozone bubbling (blue curves), and after 5 min of ozone and then 1 min of argon bubbling (green curves). The ozone concentration is determined from the maximum intensity of the Hartley band at 260 nm, assuming ε_{260nm} = 2992 M^{-1} cm^{-1}. The ozone concentration reaches ~350 μM, and the argon sparge quantitatively removes the ozone from solution.

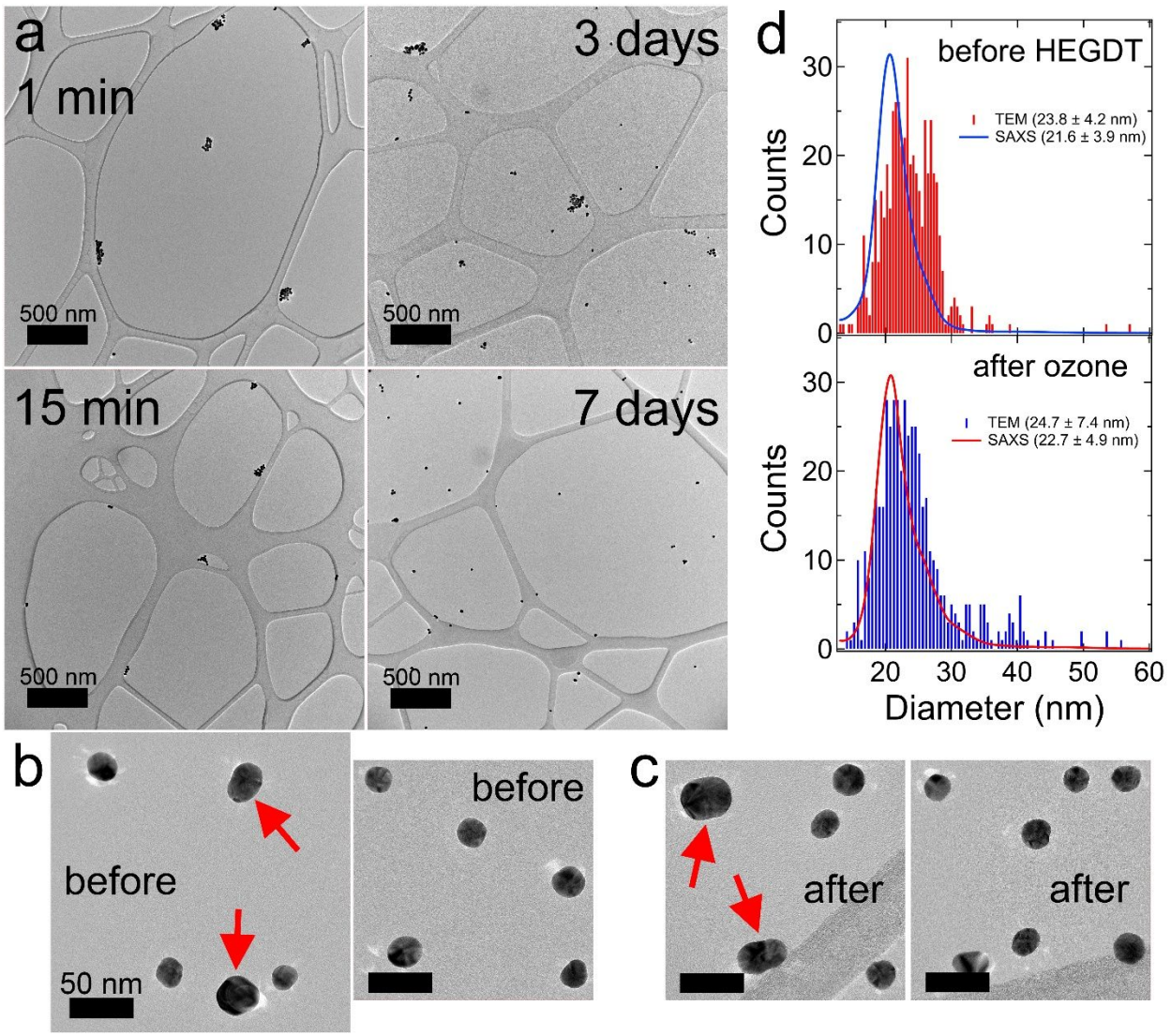

Figure S5. (a) A time series of TEM images showing the redispersion process upon ozonation of NC-HEGDT precipitates. Labels indicate the time after ozonation (5 min ozone bubbling plus 1 min argon sparge). (b-c) Typical higher-magnification images of the NCs (b) before addition of HEGDT and (c) 7 days after ozonation. The red arrows highlight several larger NCs in each type of sample. Most of these large NCs appear to be strongly-fused dimers of the smaller NCs. All samples were prepared using a technique that minimizes the artificial formation of clusters during drying of the solution on the TEM grid. (d) Size histograms of the NCs before addition of HEGDT and 7 days after ozonation, as determined by TEM (500 NCs) and colloidal small-angle X-ray scattering (SAXS). The average diameter and standard deviation are listed. The histograms show that the size of most of the NCs is unchanged after one precipitation-redispersion cycle. However, a small number of NCs do grow in size (apparent as a tail in the size distribution) as a result of the occasional fusion of neighboring NCs within the precipitates/aggregates.

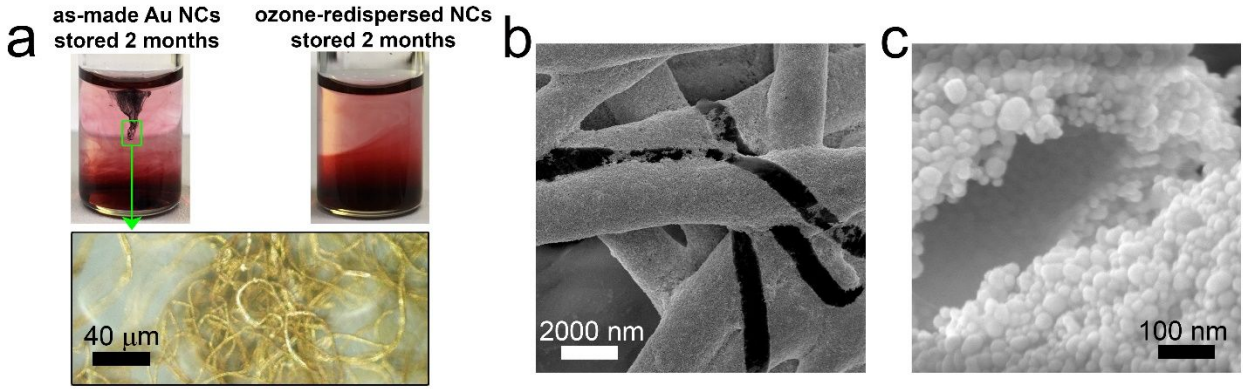

Figure S6. Ozone sterilization prevents the growth of fungus in the Au NC colloid. (a) (*upper left*) Optical image of a colloid of as-made Au NCs stored in ambient conditions for two months. A raft of filamentous fungus is visible floating in the liquid. (*bottom*) An optical microscope image shows that the filaments are coated in shells of gold. (*upper right*) Optical image of a colloid of ozone-redispersed Au NCs stored in ambient conditions for two months. No fungus is visible. The NCs are gravitationally stratified but remain fully dispersed – mild shaking of the vial results in complete homogenization of the dispersion. Ozone-redispersed NC colloids showed no fungal growth for at least two years of storage in well-sealed vials. (b) SEM image of the filaments. (c) High-magnification SEM image of a cracked filament, showing a thick coating of Au NCs surrounding an organic or hollow core.

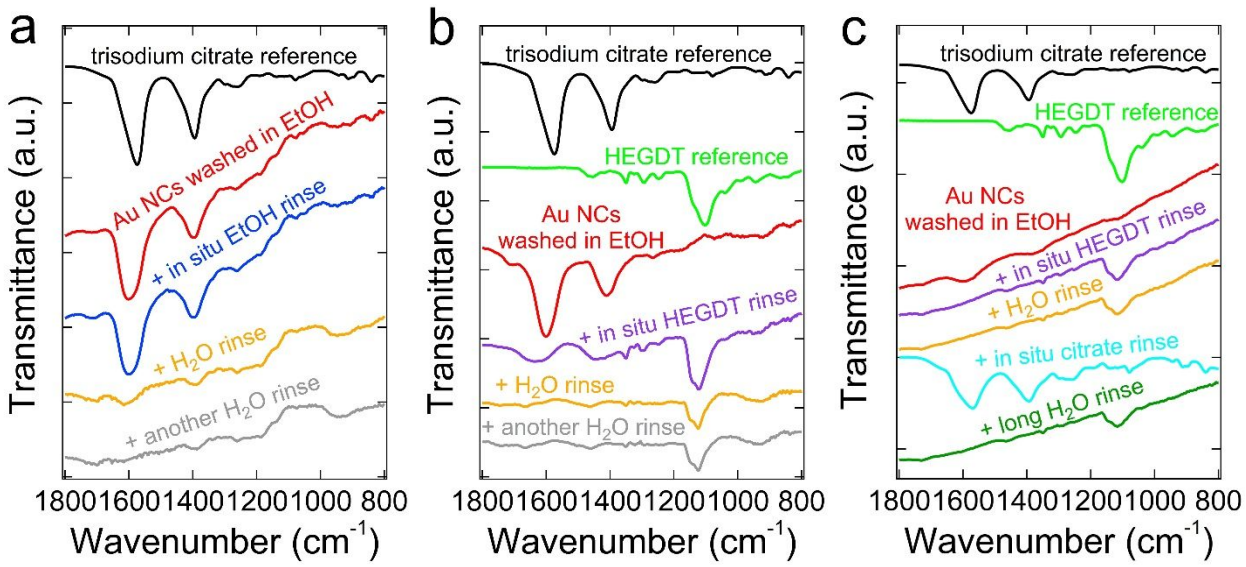

Figure S7. (a) Attenuated total reflectance FTIR spectra of citrate-capped Au NCs cleaned by four cycles of centrifugation and washing in anhydrous ethanol and then deposited onto the ATR crystal from a concentrated aqueous colloid. (*red trace*) The NCs dried on the ATR crystal. (*blue trace*) The same NC sample after rinsing with 1 mL ethanol on the ATR crystal. The citrate remains. (*orange trace*) The same sample after rinsing with 1 mL of ultrapure water. The citrate is mostly removed. (*gray trace*) The sample after a second water rinse. The citrate is totally removed. (*black trace*) A trisodium citrate powder reference spectrum. (b) ATR-FTIR data for the same type of NC sample as in (a) after drying on the ATR crystal (*red trace*), rinsing with 1 mL of 10 mM aqueous HEGDT (*purple trace*), and subsequently rinsing with ultrapure water once (*orange trace*) and twice (*gray trace*). (c) ATR-FTIR data for the same type of NC sample as in (a) after drying on the ATR crystal (*red trace*), then rinsing with 1 mL of 10 mM aqueous HEGDT (*purple trace*), rinsing with 1 mL of ultrapure water (*orange trace*), rinsing with 1 mL of 1 M trisodium citrate aqueous solution (*cyan trace*), and subsequently rinsing with ultrapure water for 30 minutes twice (*dark green trace*). Reference spectra for trisodium citrate (*black trace*) and HEGDT (*green trace*) are also shown. The strong peak in the HEGDT spectrum at 1100 cm^{-1} is from C-O (ether) stretching. We see that the aqueous HEGDT rinse removes the citrate from the NCs. Subsequent water rinsing dissolves away the non-adsorbed HEGDT, but the HEGDT that is adsorbed to the NCs is not removed by pure water or replaced by citrate. This adsorbed HEGDT can be removed by rinsing the sample in ozone-saturated water, leaving a flat and featureless FTIR spectrum (not shown). This latter result also indicates that HEGDS (the major product of HEGDT ozonation) is only weakly bound to the NCs and easily washed away by water.

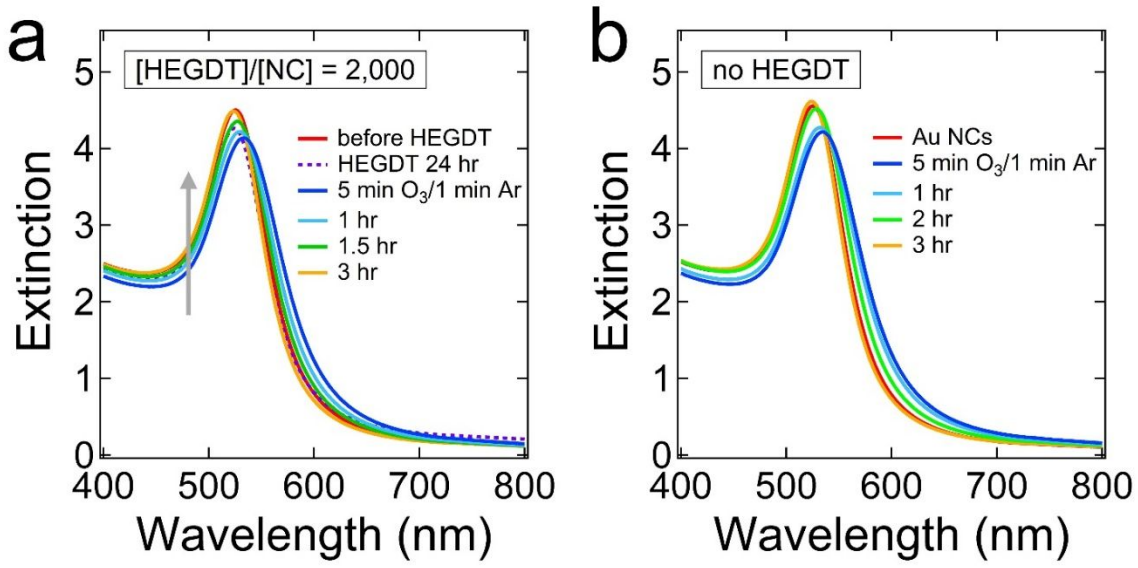

Figure S8. Effect of ozone adsorption and desorption on the optical extinction spectra of Au NCs. (a) Spectral time series upon ozonation of a NC colloid at [HEGDT]/[NC] = 2,000. Some of these data are replotted from Fig. 2d. (b) Spectral time series upon ozonation of an as-made NC colloid in the absence of HEGDT. There is an immediate redshift and diminution of the plasmonic peak due to ozone adsorption on the surface of the NCs. The spectrum recovers over ~3 hours as ozone and oxidized surface species slowly desorb from the NC surface. Note that the two time series (with and without HEGDT) are nearly identical after ozonation. We conclude that the redshift and 3-hour recovery are due to ozone and that the NC redispersion is actually very fast (minutes or less) at both small and large values of [HEGDT]/[NC].

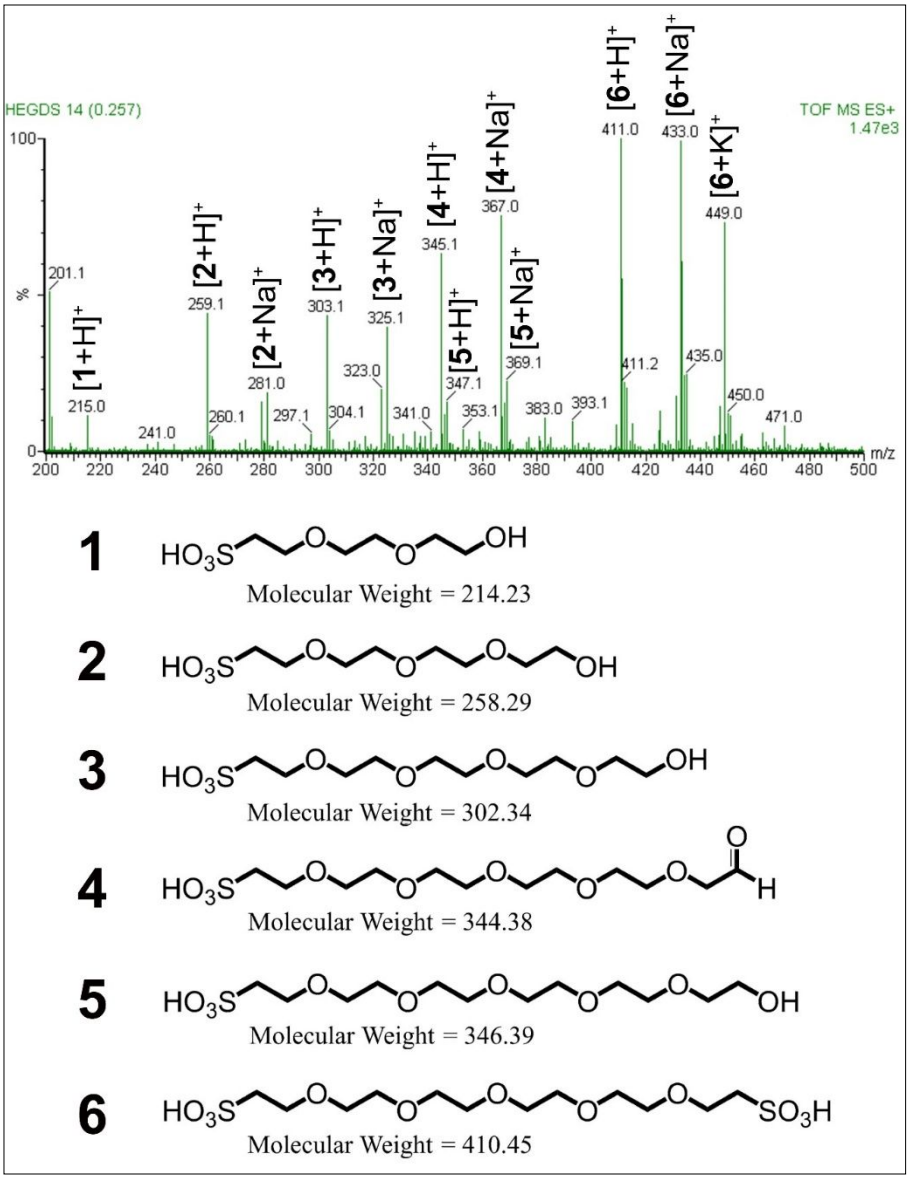

Figure S9. Electrospray ionization mass spectrum of a 10 mM solution of HEGDT in pure D_2O (1 mL sample volume) after 5 minutes of ozonation and 1 minute of argon sparging. The sample was diluted to 10 μM with CH_3OH before injection into the mass spectrometer. The major peaks index to HEGDS (**6**) and several of its hydroxy sulfonic acid and aldehyde sulfonic acid breakdown products (**1**-**5**). Peaks from HEGDT (molecular weight = 314.46) are absent, indicating quantitative oxidation of HEGDT by ozone under these conditions. The monosulfonic acid derivative (mercaptohexa(ethylene glycol) sulfonic acid) is also not observed. A control spectrum of HEGDT before ozonation showed peaks at m/z = 337.1 (assigned to $[HEGDT + Na]^+$), m/z = 299.1 (origin unknown), and m/z = 209.1 (origin unknown), but no cascade of breakdown products.

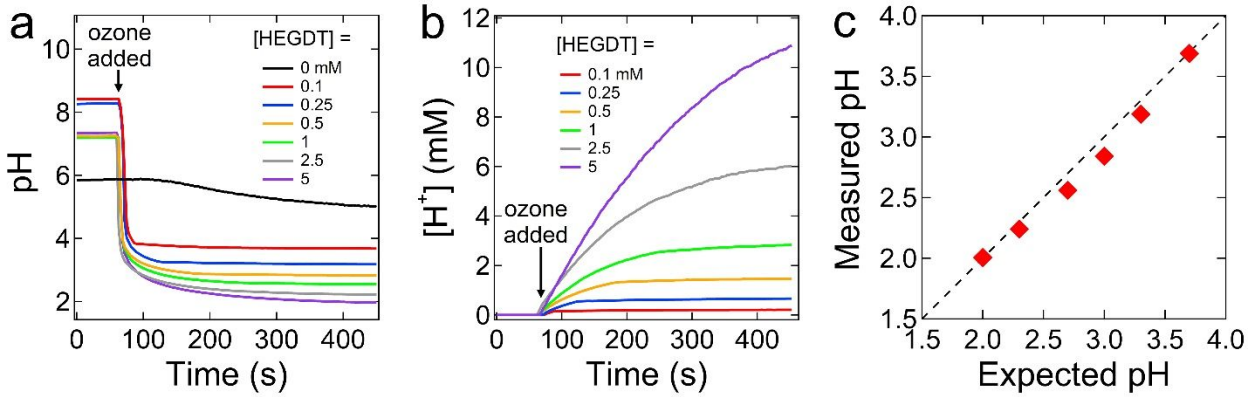

Figure S10. (a) pH versus time during the ozonation of various concentrations of HEGDT in pure H_2O. (b) $[H^+]$ as a function of time. (c) The measured pH after five minutes of ozonation versus the pH expected if ozone oxidizes each HEGDT molecule to produce two equivalents of a strong acid (e.g., HEGDS). The diagonal dashed line indicates a 1:1 correspondence. The pH change during ozonation is useful for distinguishing between possible thiol oxidation products because sulfonic acids and sulfuric acid are strong acids in water whereas aliphatic sulfinic and sulfenic acids are weak acids (typical pK_a values of ~2 and 10-12, respectively)[1,2] and other possible products (e.g., the cyclic disulfide, thiosulfinate, thiosulfonate, etc.) are nonacidic. The by-products of thiol oxidation by ozone (e.g., H_2O, H_2O_2, O_2) are also weak acids or nonacidic.[3] Note that the control experiment (ozonation of pure water, without HEGDT) shows only a small and gradual decrease in pH during ozonation.

Ozonation of NC precipitates ([HEGDT]/[NC] = 4,000) in the NC reaction mixture causes little change in pH because mM citrate acts as a buffer that prevents acidification of the solution. The pH is stable at 5.9-6.1 throughout the NC redispersion process.

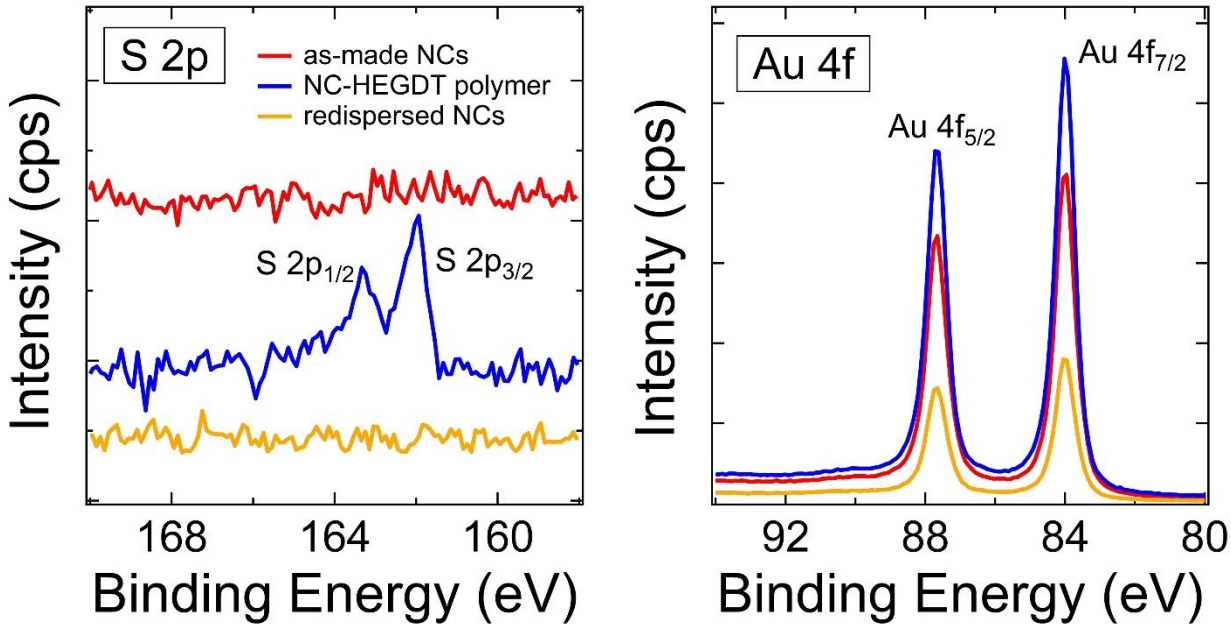

Figure S11. Sulfur 2p and gold 4f X-ray photoelectron spectra of as-made (red), HEGDT-polymerized (blue), and ozone-redispersed (orange) Au NCs on carbon tape stuck to silicon substrates. Only the spectrum of the NC-HEGDT polymer shows sulfur peaks (at 161.9 and 163.2 eV). The S 2p spectra are offset for clarity. [HEGDT]/[NC] = 4,000.

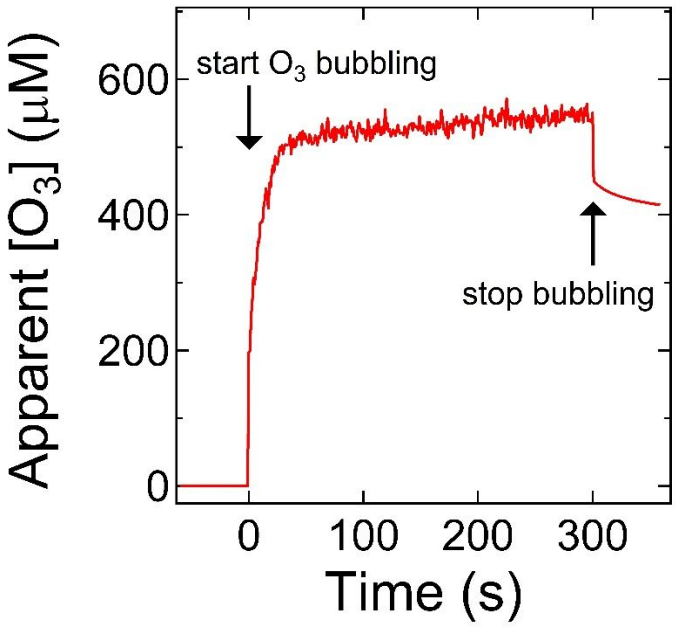

Figure S12. Apparent ozone concentration during five minutes (300 seconds) of ozone bubbling in pure water. Ozone was quantified by monitoring the optical extinction at λ = 260 nm using ε = 2992 M^{-1} cm^{-1}. Ozone reaches a nearly constant concentration in ~25 seconds. The value of $[O_3]$ is artificially high during bubbling due to light scattering and the presence of gas-phase (undissolved) O_3. We measure $[O_3] \approx 415$ μM one minute after the bubbling is stopped, which is in reasonable agreement with Fig. S4. The sample volume is 2 mL.

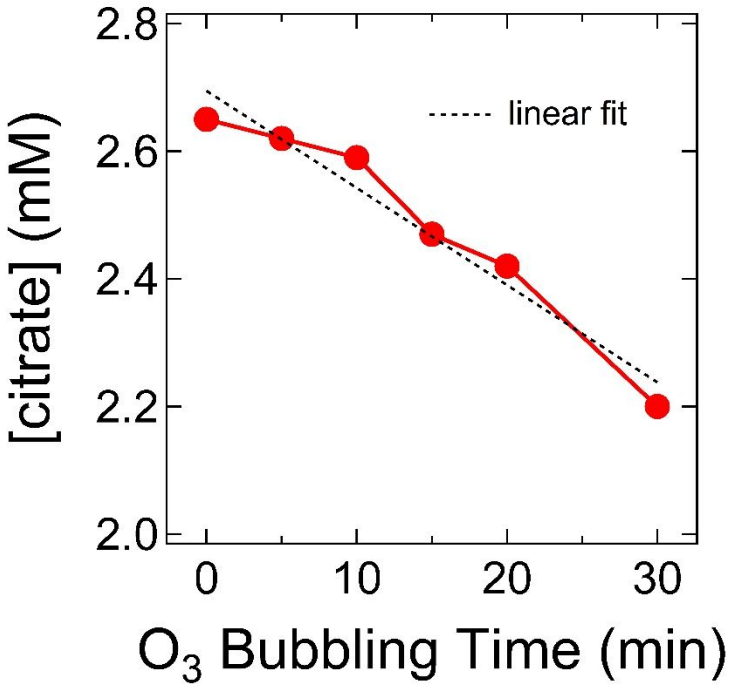

Figure S13. The concentration of citrate ion in the redispersed Au NCs as a function of ozonation time, as determined by quantitative NMR spectroscopy using an internal standard (DSS sodium salt). A linear fit of the data (dashed line) shows that the citrate concentration decreases by ~0.6% per minute of O_3 bubbling at these conditions.

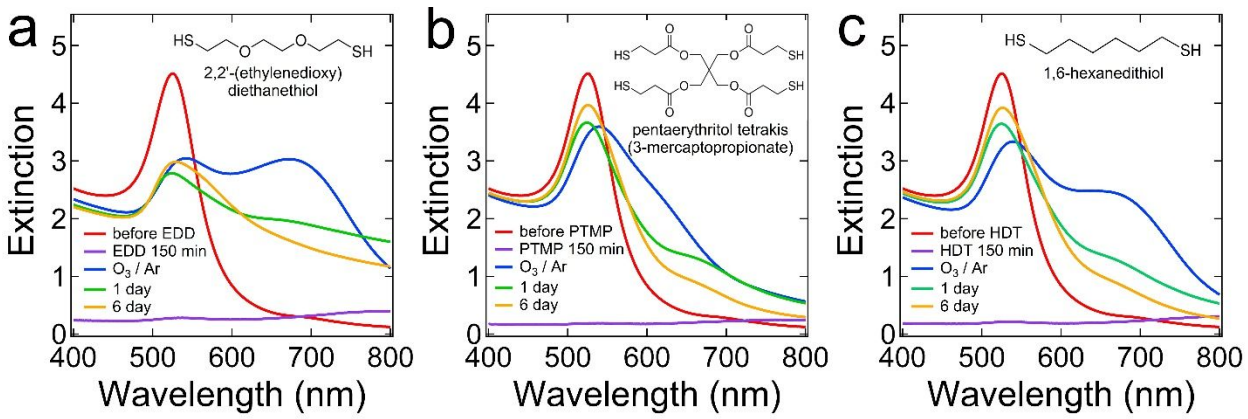

Figure S14. NC redispersion behavior for alternative thiol cross-linkers. Time series of optical extinction spectra upon five-minute ozonation of NC precipitates made by adding (a) 2,2'-(ethylenedioxy)diethanethiol, (b) pentaerythritol tetrakis(3-mercaptopropionate), or (c) 1,6-hexanedithiol to the NC reaction mixture ([thiol]/[NC] = 4,000). The molecular structure of each linker is shown as an inset. In each case, the NC precipitates totally dissolve, but the redispersion at 6 days is not as complete as it is with HEGDT (see Fig. 1). Optimization of linker concentration, ozonation time, and post-ozonation wait time is likely needed to maximize the NC redispersion for each linker.

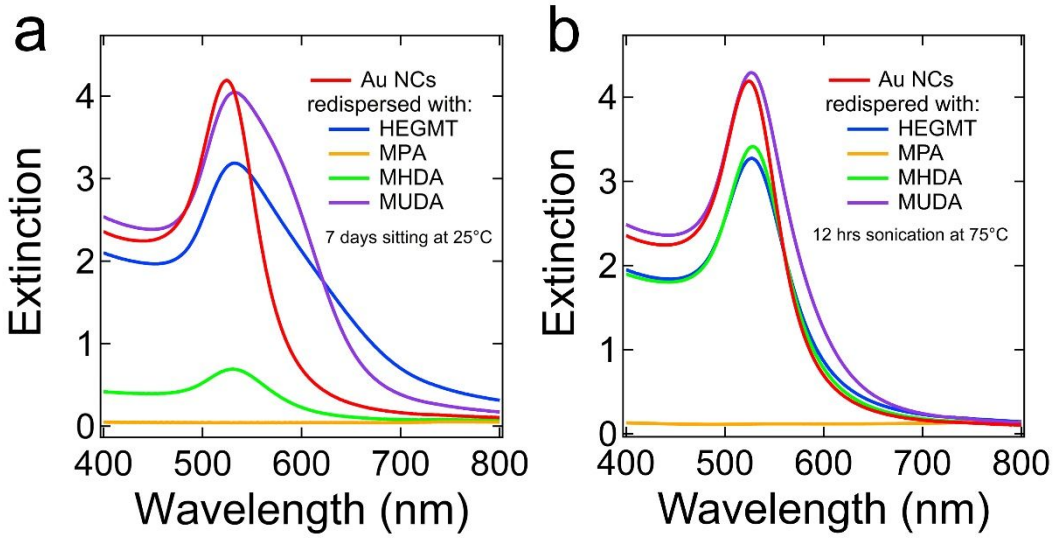

Figure S15. Redispersion of NC-HEGDT precipitates using monothiol exchange instead of ozonation. (a) Typical extinction spectra after adding 9.1 mM HEGMT, mercaptopropionic acid (MPA), 16-mercaptohexadecanoic acid (MHDA), or 11-mercaptoundecanoic acid (MUDA) to the supernatant of a NC-HEGDT precipitate, sonicating for 5 minutes, sparging with argon for 1 minute, and storing unstirred for 7 days at room temperature (all without ozone). The temperature and time mimic the conditions used for ozone-induced redispersion. (b) Spectra after addition of the various monothiols and sonication for 12 hours at 75°C (no ozone). These temperature and sonication conditions are much more extreme than the conditions used for ozonation. In all experiments, [monothiol]/[HEGDT] = 1,000. Note that MHDA and MUDA were dissolved in ethanol and formed an emulsion upon injection into the aqueous supernatant, so the MHDA- and MUDA-treated samples were passed through a 200 nm syringe filter to minimize light scattering prior to measurement. An unknown amount of NC aggregates, single NCs, and water was removed from these samples by filtering. Therefore, the spectra of the MHDA and MUDA samples are distorted, with unreliable peak amplitudes and artificially small low-energy absorption tails (the samples actually contain more NC aggregates than the data suggest).

References

[1] Oea, S.; Doi, J. *Organic Sulfur Chemistry: Structure and Mechanism.* CRC Press: Boca Raton, Florida, 1991.

[2] Block, E. *Garlic and Other Alliums: The Lore and the Science*. Royal Society of Chemistry: Cambridge, U.K., 2010.

[3] Staehelln, J.; Hoigné, J. Decomposition of ozone in water in the presence of organic solutes acting as promoters and inhibitors of radical chain reactions. *Environ. Sci. Technol*. **1985**, *19*, 1206-1213.